**Title:**

# Temperature Dependence of Structural Dynamics at the Catalytic Cofactor of [FeFe]-hydrogenase

Author(s):

Sven T. Stripp, Stefan Mebs, and Michael Haumann



Citation:

"Inorg. Chem. 2020, 59, 22, 16474–16488 ; https://doi.org/10.1021/acs.macromol.0c00138"

**Temperature dependence of structural dynamics at the active site of [FeFe]-hydrogenase**

Sven T. Stripp, Stefan Mebs, Michael Haumann*

Freie Universität Berlin, Physics Department, Arnimallee 14, 14195 Berlin, Germany

**Correspondence to:*

Dr. Michael Haumann, Freie Universität Berlin, Fachbereich Physik, Arnimallee 14, 14195 Berlin, Germany,

Email: michael.haumann@fu-berlin.de

**Running title:** Temperature dependence of the H-cluster structure

**Keywords:** [FeFe]-hydrogenase, catalytic cofactor, infrared spectroscopy, X-ray absorption spectroscopy, structural dynamics

**Abbreviations:** ATR FTIR, attenuated total reflection Fourier-transform infrared spectroscopy; DFT, density functional theory; EPR, electron paramagnetic resonance spectroscopy; EXAFS, extended X-ray absorption fine structure; FWHM, full width at half maximum; NFS, nuclear forward ($^{57}$Fe X-ray) scattering; NRVS, nuclear resonance ($^{57}$Fe X-ray) vibrational spectroscopy; PCET, proton-coupled electron transfer; QM/MM, quantum mechanics / molecular mechanics calculations; XANES, X-ray absorption near-edge structure; XAS, X-ray absorption spectroscopy

**Abstract**

[FeFe]-hydrogenases are nature´s blueprint for efficient hydrogen turnover. Understanding their enzymatic mechanism may improve technological $H_2$ fuel generation. The active-site cofactor (H-cluster) consists of a [4Fe-4S] cluster ($[4Fe]_H$), cysteine-linked to a diiron site ($[2Fe]_H$) carrying an azadithiolate group (adt), terminal cyanide and carbon monoxide ligands, and a bridging carbon monoxide ($\mu$CO) in the oxidized protein (**Hox**). Recently, the debate on the structure of reduced H-cluster states was intensified by the assignment of new species under cryogenic conditions. We investigated temperature effects (4-300 K) in infrared (IR) and X-ray absorption spectroscopy (XAS) data of [FeFe]-hydrogenases using fit analyses and quantum chemical calculations. Infrared data from our laboratory and literature sources suggest that reduced, room-temperature states with a bridging hydride ($\mu H^-$, in **Hred** and **Hsred**) or with an additional proton at $[4Fe]_H$ (**Hred´**) or at the distal iron of $[2Fe]_H$ (**Hhyd**) are largely replaced by cryogenic-temperature states that hold a $\mu$CO, lack $[4Fe]_H$ protonation, and bind an additional proton at the adt nitrogen (**HredH$^+$**, **HsredH$^+$**). XAS revealed the atomic coordinate dispersion (i.e., the Debye-Waller parameter, $2\sigma^2$) of the iron-ligand bonds and Fe-Fe distances in the oxidized and reduced H-cluster. $2\sigma^2$ showed a temperature dependence typical for the so-called protein-glass transition, with small changes below ~200 K and a pronounced increase above this “breakpoint”. This behavior is attributed to the freezing-out of larger-scale anharmonic motions of amino-acid sidechains and water species. We propose that protonation at $[4Fe]_H$ as well as ligand rearrangement and $\mu H^-$ binding at $[2Fe]_H$ are impaired due to restricted molecular mobility at cryogenic temperatures so that protonation can be biased to the adt. We conclude that a H-cluster with a $\mu$CO, selective $[4Fe]_H$ or $[2Fe]_H$ protonation, and catalytic proton transfer via the adt facilitates efficient $H_2$ conversion in [FeFe]-hydrogenase.

## Introduction

[FeFe]-hydrogenase enzymes catalyze efficient dihydrogen ($H_2$) conversion at a six-iron cofactor, the so-called H-cluster.[1-5] The mechanism of this active site needs to be understood to aid the improvement of synthetic $H_2$ conversion catalysts. Crystal structures of [FeFe]-hydrogenases have revealed the configuration of the oxidized H-cluster, **Hox** (Fig. 1).[6-8]

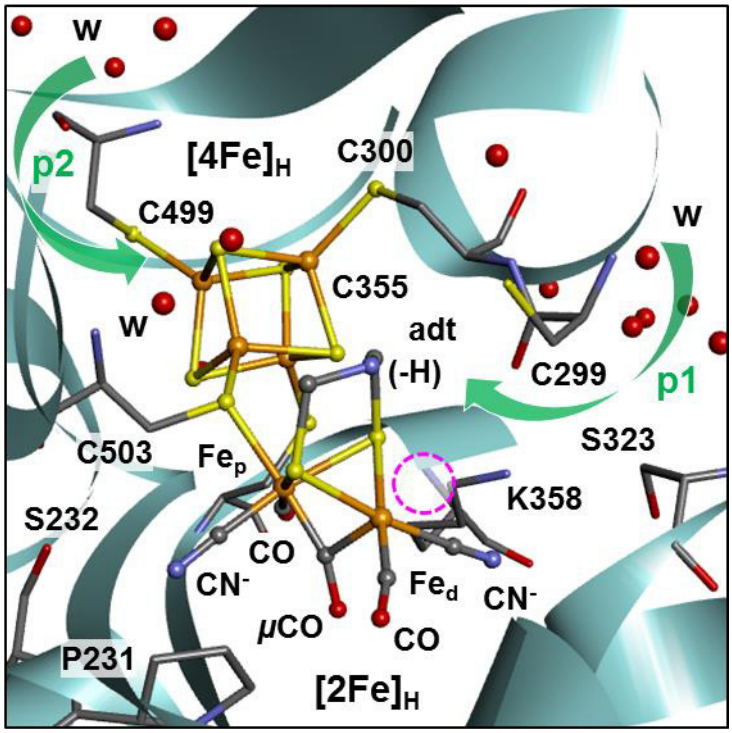


***Figure 1:*** *Crystal structure of the H-cluster. The structure is for CpI [FeFe]-hydrogenase and assigned to the* ***Hox*** *state (PDB-ID 4XDC, 1.63 Å resolution).[8] Orientations of terminal or bridging $CN^-$/CO ligands are annotated;[9] $Fe_{p,d}$, proximal or distal iron atom of the diiron site; adt = azadithiolate ligand ($NH(SCH_2)_2$)[10]; the magenta circle marks the open coordination site at $Fe_d$; w denotes water molecules conserved in many structures and involved in two proton transfer pathways to $[2Fe]_H$ (p1, via, e.g., Cys299 and Ser323) or $[4Fe]_H$ (p2).[11-13] Lys358, Pro231, and Ser232 (Ala in CrHydA1) contribute to hydrogen-bonding of the $CN^-$ ligands.*

Almost three decades of spectroscopic analyses on the catalytic [FeFe]-hydrogenases from bacteria (*Clostridium acetobutylicum, Ca*I*; Clostridium pasteurianum*, *Cp*I; *Desulfovibrio desulfuricans*, *Dd*H) or green algae (*Chlamydomonas reinhardtii*, *Cr*HydA1) have led to the postulation of about 20 states of the H-cluster until today (Tables 1, S1, S2).[1-4, 14-15] However, crystal structures of pure H-cluster states other than **Hox** and **Hox-CO** are not available. This sparked considerable debate on the structure of many of the H-cluster species and led to partially incompatible schemes for the catalytic cycle of $H_2$ conversion (refs.[2, 16-18] show recent versions). It is the focus of this study to gain further insight into the structure and involvement of H-cluster states in the catalytic cycle. Moreover, we suggest a unified nomenclature of H-cluster states.

**Table 1:** IR signatures of H-cluster states.

| state[a] | infrared frequencies [$cm^{-1}$] | | | | | | ref. |
|---|---|---|---|---|---|---|---|
| | $CN^-$ | | CO | | | $\mu$CO | |
| **Hox** | 2089 | 2072 | - | 1964 | 1040 | 1804 | this work |
| **Hred´** | 2086±3 | 2067±5 | - | 1962±2 | 1934±2 | 1790±3 | [11, 16, 19] |
| **Hred** | 2073 | 2034 | 1961 | 1915 | 1891 | - | this work |
| | 2075±4 | 2037±4 | 1964±3 | 1915±1 | 1892±2 | - | [12, 15-16, 19-23] |
| **Hred$_{LT}$** | 2078±4 | 2038±3 | - | 1918±4 | 1895±4 | 1809±8 | [16-18] |
| **Hred*** | 2055 | 2022 | - | 1894 | 1871 | 1763 | [24] |
| **Hsred** | 2069 | 2027 | 1954 | 1918 | 1883 | - | this work |
| | 2068±2 | 2029±3 | 1956±3 | 1917±4 | 1882±2 | - | [12, 19, 21-22, 25] |
| **Hsred$_{LT}$** | 2072±2 | 2030±3 | - | 1919±4 | 1882±1 | 1800±1 | [16-18] |
| **Hsred*** | 2047 | 2013 | - | 1900 | 1861 | 1751 | [24] |
| **Hhyd** | 2085±3 | 2073±5 | - | 1981±3 | 1964±4 | 1857±4 | [12, 16-17, 26-27] |
| **Hhyd$_{LT}$** | 2087 | 2078 | - | 1972 | 1954 | 1851 | [18] |

[a]Annotations follow earlier or here defined nomenclatures (**Hred´** was denoted Hred in refs.[16, 19, 22], **Hred/Hsred** were earlier denoted **HredH$^+$/HsredH$^+$** in refs.[16-19, 22, 25]; no subscript, room temperature data; LT, low temperature data assigned now to **HredH$^+$/HsredH$^+$** in refs.[17-18] or to a Hhyd-like species (**Hhyd:red**) in ref.[18]. *, data for a regulatory [FeFe]-hydrogenase,[24] otherwise catalytic enzymes. This work, data for *Cr*HydA1 (**Hox** frequencies in other enzymes are ±5 $cm^{-1}$ similar). Given frequency variations represent the full range for different enzymes (Table S2 lists the individual frequencies, Table S1 shows IR data of further H-cluster states).

The H-cluster consists of a [4Fe-4S] cluster, $[4Fe]_H$, which is connected by a cysteine residue to a diiron complex, $[2Fe]_H$, that carries two cyanide ($CN^-$) and three carbon monoxide (CO) ligands as well as a bridging azadithiolate group (adt = $(SCH_2)_2NH$), Fig. 1). In **Hox**, one CO ($\mu$CO) binds in the $Fe_p$-$Fe_d$ bridging position (p/d = proximal/distal iron of $[2Fe]_H$ relative to $[4Fe]_H$), which stabilizes an open coordination site at $Fe_d$. A fourth CO binds at $[2Fe]_H$ in the oxidized CO-inhibited state (**Hox-CO**). Crystallographic, spectroscopic, and computational analyses have suggested that reduction of the H-cluster by one or two electrons is coupled to structural changes at $[2Fe]_H$ and is associated with protonation at one or both sub-complexes. Several $1e^-$ (**Hred´**, **Hred**) or $2e^-$ (**Hsred**, **Hhyd**) reduced H-cluster states were assigned, largely based on infrared band signatures due to the $CN^-$ and CO ligand stretching vibrations.[1-4, 15, 17-18, 28] The debate on the involvement of H-cluster species in the catalytic cycle is primarily due to the lack of consent on the properties of certain reduced states. Recently proposed structures of (single-electron) reduced H-cluster species from our or other author´s work are summarized in Scheme 1 for clarity.

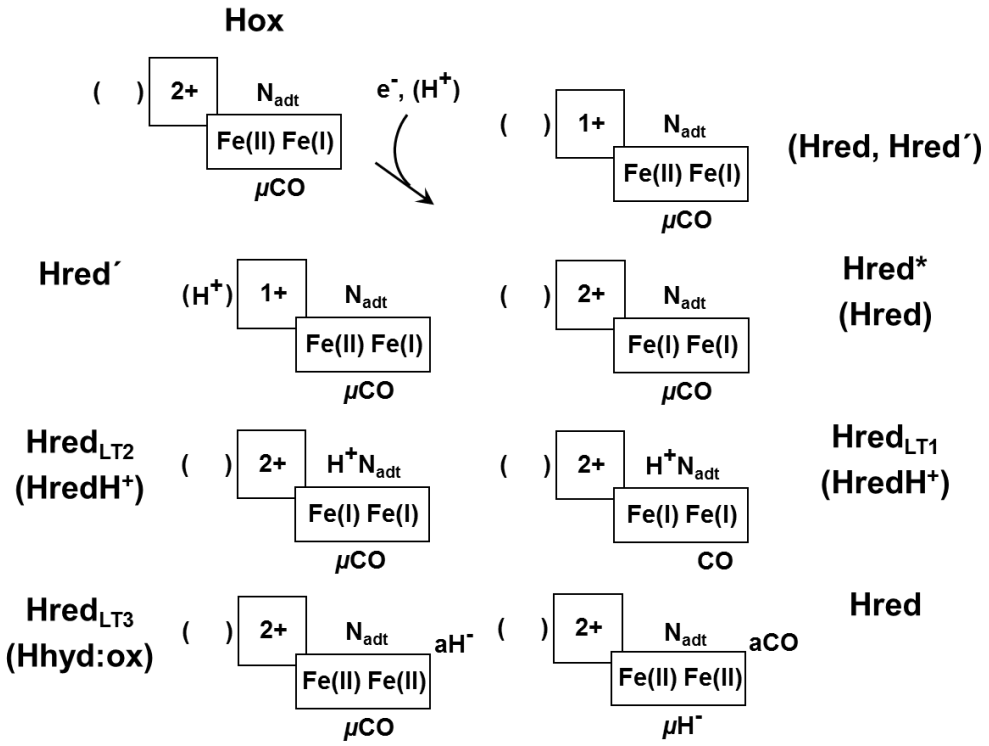

***Scheme 1:*** *Proposed configurations of the 1e⁻ reduced H-cluster vs.* ***Hox****. Respective proposed 2e⁻ reduced species are mostly derived by reduction of [4Fe$_H$]. State annotations as used in the present paper (LT, low temperature) and our previous publications[2, 11, 20-21, 29-30] or in recent work by other authors[16-18, 24, 31] (in parenthesis) are compared (see also Tables 1, S2). Formal hydride and CO species bind at [2Fe]$_H$ in bridging position (μ) or apically (a) at Fe$_d$. For further details see the text.*

For **Hhyd**, a structure with a terminal hydride bound at $Fe_d$ was consistently suggested (Fig. 1).[12, 16-17, 26, 29, 32] For **Hred´**, the IR signature shows a $\mu$CO at $[2Fe]_H$ and the ~60 mV/pH redox potential decrease in the Pourbaix diagram suggests proton-coupled reduction, which we assigned to a protonation at a cysteine ligand of $[4Fe]_H$ (similar to **Hhyd**).[11, 19, 30] For **Hred**, early IR studies[12, 19, 21-22, 25] suggested the absence of a $\mu$CO at $[2Fe]_H$ and a proton at the adt nitrogen (N(adt)).[19, 25, 33] An apparently semi-bridging CO was among the crystallographic changes in reduced *Dd*H enzyme where the H-cluster states were not verified (Scheme 1).[23, 34] For **Hsred**, the lack of a low-frequency CO band and the large frequency difference of the $CN^-$ bands[15] prompted the assignment of **Hsred** to a similar structure lacking a true $\mu$CO with a reduced $[4Fe]_H$ cluster in addition.[19, 25, 33] In contrast, we have assigned **Hsred** to a structure with reduced $[4Fe]_H$ and $[2Fe]_H$ sub-complexes, but with a bridging hydride ($\mu H^-$) at $[2Fe]_H$, based on correlation of IR, X-ray spectroscopy, and quantum-chemical computations.[21, 35] Following similar reasoning, e.g., a similar IR signature for **Hred** and **Hsred** (Tables 1, S2),[15] **Hred** was assigned to a structure carrying a $\mu H^-$ at $[2Fe]_H$ (Scheme 1).[20-21, 29, 35] Further models for **Hred** were suggested by other authors (Scheme 1).[31] Our computational analyses of IR and NRVS data, as well as $^{13}CO$ isotope labeling experiments clearly supported the absence of a $\mu$CO in **Hred** and **Hsred** and rendered alternative structures, e.g., with a non-bridging CO and N(adt) protonation unlikely.[20-21]

A recent twist in the interpretation of the **Hred** and **Hsred** structures has emerged from studies of temperature and light effects on the H-cluster. It was found that upon decreasing the temperature to cryogenic levels under strongly reducing conditions, H-cluster states were populated, which show IR bands similar to **Hred** or **Hsred** except for an additional low-frequency band (ca. 1800 – 1820 $cm^{-1}$) attributed to a $\mu$CO ligand (Tables 1, S2).[16-18] In the following, we denote such species as low-temperature (LT) states, i.e., $\mathbf{Hred_{LT}}$ and $\mathbf{Hsred_{LT}}$ (Scheme 1). Further experiments suggested that the usual IR signatures of **Hred** and **Hsred** were regained at the expense of $\mathbf{Hred_{LT}}$ and $\mathbf{Hsred_{LT}}$ upon rising the temperature above 200 K.[16] Interestingly, $\mathbf{Hred_{LT}}$/$\mathbf{Hsred_{LT}}$ were converted upon low-temperature illumination to states resembling **Hhyd**, but with $\mu$CO bands at ~10 $cm^{-1}$ higher or lower frequencies. The signatures were assigned to more oxidized or reduced hydride species (**Hhyd:ox**, **Hhyd:red**) (Tables 1, S2; Scheme 1).[18] Furthermore, in a sensory [FeFe]-hydrogenase, states with IR signatures including $\mu$CO bands at particularly low frequencies (1750 – 1760 $cm^{-1}$) were observed to prevail under reducing conditions even at room temperature (**Hred***, **Hsred***; Tables 1, S2; Scheme 1).[24]

Surprisingly, the above findings have prompted the re-assignment also of the room-temperature reduced states **Hred** and **Hsred** to H-cluster species with a $\mu$CO ligand (Scheme 1).[16-18] This re-assignment was made irrespective of the apparent absence of a $\mu$CO IR-band of **Hred** and **Hsred** at ambient temperatures and of the alterations at the reduced H-cluster in the crystal structure,[23, 34] which was one reason for the original semi-bridging CO proposal. Birrell et al. speculated that the apparent absence of a $\mu$CO band was due to band broadening at room temperature so that it escapes detection, while for the terminal CO/$CN^-$ bands only minor broadening was reported in a 4-300 K range.[17] Interestingly, a recent crystallographic study on the *Cp*I enzyme revealed two apparent configurations of the active site, showing different orientations of the sidechains of Ser357 neighboring $[4Fe]_H$ and Met353 close to $[2Fe]_H$, but

both bearing a $\mu$CO ligand.[36] These species were attributed to oxidized (**Hox**) or reduced (**HredH$^+$**) H-cluster states since their relative occupancies varied due to X-ray photoreduction or dithionite treatment of the crystals.[36] These attributions may be debatable because the oxidized structure showed an additional atom (modeled as oxygen) bound at ~2.65 Å to the apical site of $Fe_d$, at variance with other **Hox** structures with an apical vacancy,[8] which is more similar to $O_2$- or S-inhibited H-cluster species,[29, 37] while the (photo)reduced crystals as monitored in the diffraction data collection at 100 K may comprise several H-cluster species that carry a $\mu$CO (e.g., **Hred´**, **HredH$^+$**, **Hhyd**) with their populations depending on the sample reduction source and temperature (see below). We note that protons at, e.g., the adt nitrogen, the $[2Fe]_H$ iron sites, or the $[4Fe]_H$ complex were not resolved in the diffraction data of the (partly) reduced crystals. The seemingly inconsistent and/or incomplete assignment of the reduced species prompted us to study the temperature dependence of the H-cluster dynamics using quantitative evaluation of FTIR spectra as obtained here or in the literature, as well as X-ray absorption spectroscopy (XAS) at the Fe K-edge.

Using the model [FeFe]-hydrogenase *Cr*HydA1, we found that the vibrational dynamics at the H-cluster displays so-called protein-glass transition behavior,[38-40] meaning that the atomic coordinate deviation decreases to a "breakpoint" at ~200 K and remains rather constant at lower temperatures. Reported IR spectra of reduced [FeFe]-hydrogenases apparently comprise a similar temperature dependence.[17] We interpret the experimental and computational findings as the freezing-out of protonation at the $[4Fe]_H$ sub-cluster and of ligand reorientation at the diiron site upon reduction, leading to preferential $[2Fe]_H$ reduction and protonation at the azadithiolate headgroup or the distal iron center, as well as to $\mu$CO stabilization at cryogenic temperatures.

## Materials and Methods

***HydA1 protein sample preparation.*** The preparation of apo-*Cr*HydA1 was carried out and its purity was assayed using published protocols.[20, 29] $(Et_4N)_2[Fe_2(adt)(CO)_4(CN)_2]$ ($2Fe_{adt}$) was synthesized according to literature protocols with minor modifications and its purity assayed as outlined earlier.[8, 41-42] Quantitative in-vitro reconstitution of apo-HYDA1 with the $2Fe_{adt}$ complex was carried out as previously described.[8, 43-45] All protein preparation and handling procedures were carried out under strictly anoxic conditions and dim light at room temperature. *Cr*HydA1 holo-protein solution samples were prepared similar as reported earlier under FTIR control, i.e., for ~1 µl aliquots of samples FTIR spectra were collected every ~5 min during the gassing procedures.[20, 29] Extensive (~30 min) flushing with humidified $N_2$ gas of *Cr*HydA1 solutions (~30 µL, ~2 mM, buffer at pH 8) resulted in near-quantitative **Hox** population while flushing with humidified $H_2$ gas resulted in dominant **Hred´/Hred** populations, as quantified by FTIR (Fig. S2). Samples were transferred to holders for XAS under similar atmospheres and rapidly frozen (~3 s) in liquid nitrogen in the glovebox.

***Infrared spectroscopy.*** ATR FTIR spectroscopy, employing hydrogenase protein film conditioning via exposure to varying gas mixtures or using an electrochemical approach, was carried out using our earlier described experimental set-up and procedures. [9, 11, 30, 46] Simulation of FTIR spectra as derived here or from literature reports was carried out using in-house curve-fitting software.[9, 21, 29] Further details are given in the Supporting Information text and data files.

***X-ray absorption spectroscopy.*** XAS at the Fe K-edge was performed at beamline KMC-3 at the BESSY-II synchrotron (Helmholtz Center Berlin, Germany; 300 mA top-up mode of the storage ring) as described earlier,[47-49] using a set-up including a Si[111] double-crystal monochromator, a 13-element energy-resolving Si-drift detector (RaySpec), and DXP-XMAP pulse-processing electronics (XIA). Samples were held in a liquid-helium cryostat (Oxford) at

temperatures ranging between about 20-300 K. The sample temperature was adjusted via the He-flow/heating control system of the cryostat and was measured via a sensor close to the holder on the cryostat rod. The energy axis of the monochromator was calibrated (accuracy ±0.1 eV) using the K-edge spectrum of an iron metal foil (fitted reference energy of 7112 eV in the first derivative spectrum). The spot size on the samples was ca. 0.5 x 1.5 mm (vertical x horizontal) as set by a focusing mirror and slits. Several non-overlapping spots of the sample were moved into the X-ray beam by computerized positioning of the rod (vertical) or whole cryostat (horizontal) and X-ray fluorescence spectra were collected using a continuous monochromator-scan mode (scan duration ~10 min). Up to 6 scans to k = 14.2 $Å^{-1}$ per temperature were averaged (1-2 scans per sample spot) for signal-to-noise ratio improvement. XAS data were processed (dead-time correction, background subtraction, normalization) to yield XANES and EXAFS spectra using our earlier described procedures and in-house software.[47-50] $k^3$-weighted EXAFS spectra were simulated with in-house software and phase functions from FEFF9 ($S_0^2$ = 0.8).[51-52]

***Quantum chemical calculations.*** Calculations were carried out on the large-scale computer facilities of the Freie Universität Berlin. They involved model structures as constructed using the crystal structure of oxidized [FeFe]-hydrogenase *Cp*I (PDB entry 4XDC, 1.63 Å resolution[8]) as a starting point, as described in detail earlier (Fig. S15, SI coordinates file).[20-21, 29] For large model structures (truncated *Cp*I structure resembling the structure of apo-HydA1 and lacking accessory FeS clusters), a quantum mechanics/molecular mechanics (QM/MM) approach including ONIOM[53-54] and the Universal Force Field as implemented in Gaussian09[55] were used for the MM treatment of the protein environment (low-layer) and the TPSSh[56] or BP86[57] functional was used for the QM core (high-layer including the H-cluster) for unconstraint geometry-optimization. For small model structures (including the H-cluster, cysteine ligands were represented by $SCH_2CH_3$ groups), DFT was applied for geometry-optimization (TPSSh

or BP86 functional). Both approaches involved the TZVP basis set.[58] A broken-symmetry approach and proper assignment of molecular fragments were used for calculation of anti-ferromagnetic spin couplings.[21] For **Hox**, the total spin multiplicity (M = 2S + 1) was 2 and the total charge of the H-cluster was −3. For other species, multiplicities and charges reflected the number of added electrons and protons. Vibrational frequencies were derived from normal mode analysis of relaxed structures using Gaussian09, which yielded IR stick spectra that were broadened by pseudo-Voigt functions (40 % Lorentzian and 60 % Gaussian characters) with FWHM values similar to the experimental data.[20-21, 29]

## Results

***Analysis of infrared spectra at room temperature and cryogenic temperatures.*** IR spectra of different H-cluster states as obtained here or in earlier publications were quantitatively evaluated for a consistent assignment of the $CN^-$/CO band signatures. First, **Hox**, **Hred**, and **Hsred** were enriched in *Cr*HydA1 protein films using an ATR FTIR spectro-electrochemistry approach (Fig. 2).[30] Under mildly acidic conditions (pH ~5) and in the absence of a reductant (i.e., sodium dithionite), **Hox** was populated at a potential of -300 mV whereas **Hred** or **Hsred** were populated at potentials of -550 mV or -750 mV, respectively. The resulting FTIR spectra at room temperature (~298 K) revealed clear dominance of the CO/$CN^-$ bands of **Hox**, **Hred**, or **Hsred** (Fig. 2A).

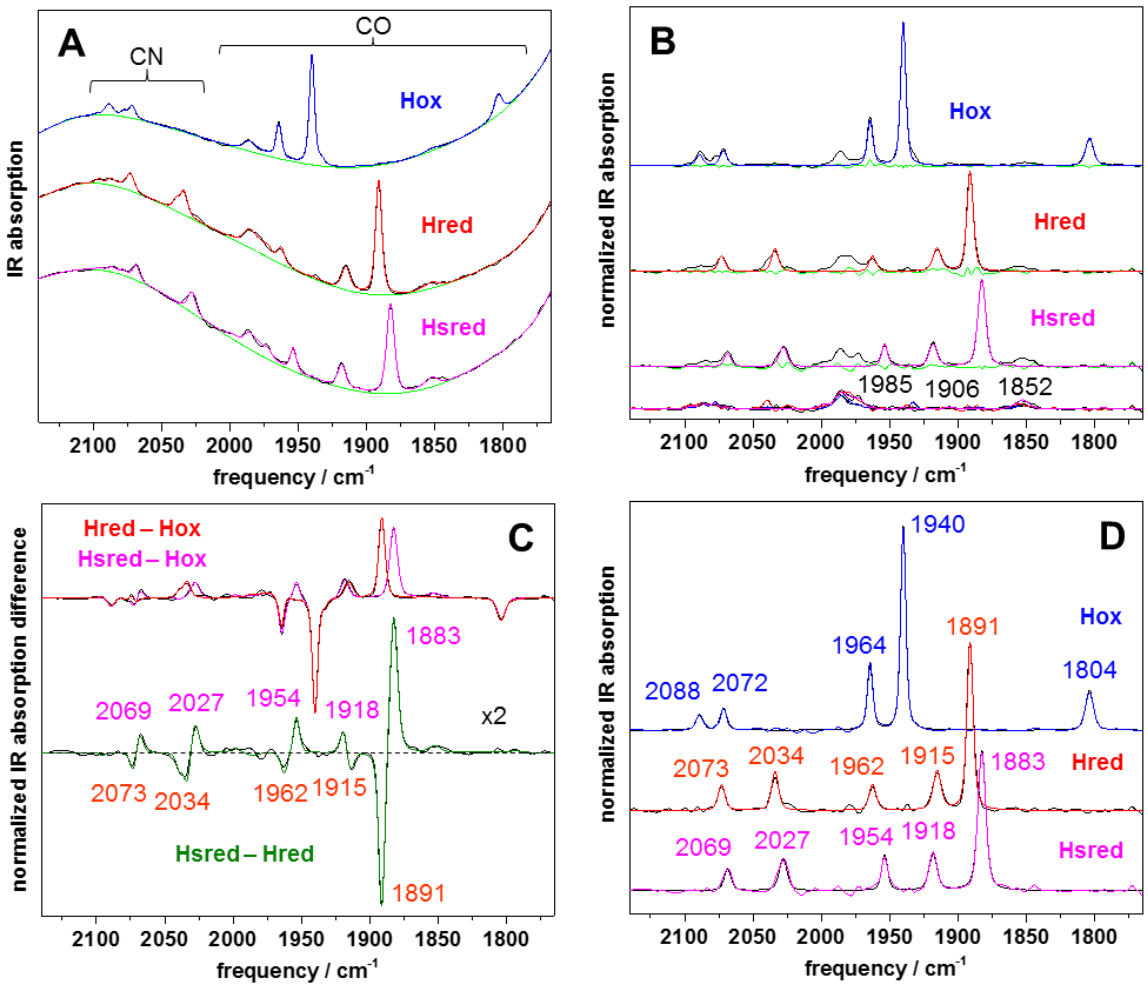


***Figure 2:*** *ATR FTIR spectra of CrHydA1. H-cluster states were electrochemically enriched and spectra analyzed with a joint-fit. (A) Raw spectra in the CO/CN⁻ band region (experimental data, black lines; fit curves, blue/red/magenta lines; baselines, green lines; spectra were vertically stacked for clarity). Fit parameters are listed in Table S3. (B) Spectra after background subtraction and normalization (experimental data, black lines; fit curves for the dominant H-cluster states, blue/red/magenta lines; residuals for fit curves as in (A), green lines). The bottom traces show experimental and fitted spectra accounting for the further H-cluster states, e.g., minor unbound $2Fe_{adt}$.[59] (C) FTIR difference spectra calculated from data in (B). Band frequencies of* ***Hox****,* ***Hred****, or* ***Hsred*** *are indicated. The following state populations (in %) were derived (****Hox/Hred/Hsred/Hhyd****/Hx/$2Fe_{adt}$, Hx is mainly* ***Hox-CO*** *and* ***Hred´****) in the samples:* ***Hox****, 76/2/1/2/5/14;* ***Hred****, 1/67/0/7/5/20;* ***Hsred****, 0/1/68/8/3/18. (D) Normalized spectra of pure* ***Hox****,* ***Hred****, and* ***Hsred*** *after subtraction of other contributions from spectra in (B) (experimental data, black lines; fit curves, blue/red/magenta lines).*

The spectra were analyzed using a joint-fit procedure (Table S3), which resulted in a quantitative description with small residuals and clear identification of the IR signatures of **Hred** and **Hsred**, besides of minor spectral contributions, e.g., from unbound $2Fe_{adt}$ (Fig. 2B). These IR signatures were well visible in the difference spectra, in particular the **Hsred** – **Hred** difference clearly highlights the contributions from all five $CN^-$/CO bands, with no significant spectral differences in the low-frequency $\mu$CO region (around 1790 – 1825 $cm^{-1}$, Fig. 2C). Finally, this approach resulted in IR spectra of the pure **Hred** and **Hsred** species, which reveal relative band features very similar to our and other authors earlier reports for *Cr*HydA1, *Ca*I, *Cp*I, and *Dd*H [FeFe]-hydrogenases at room temperature, clearly lacking a $\mu$CO band (Fig. 2D). Tables 1, S2, S3 and Fig. S1 summarize IR data for various [FeFe]-hydrogenases from literature compared to our present *Cr*HydA1 results, which reveals only minor frequency variations. In conclusion, at room temperature the H-cluster in **Hred** and **Hsred** does not possess a $\mu$CO ligand at $[2Fe]_H$ so that the three CO ligands are bound in terminal positions at $Fe_p$ or $Fe_d$. We compare the room temperature FTIR spectra of the pure **Hred** and **Hsred** states of *Cr*HydA1 to spectra, e.g., of low temperature species as derived from literature data in Fig. 3 (see below).

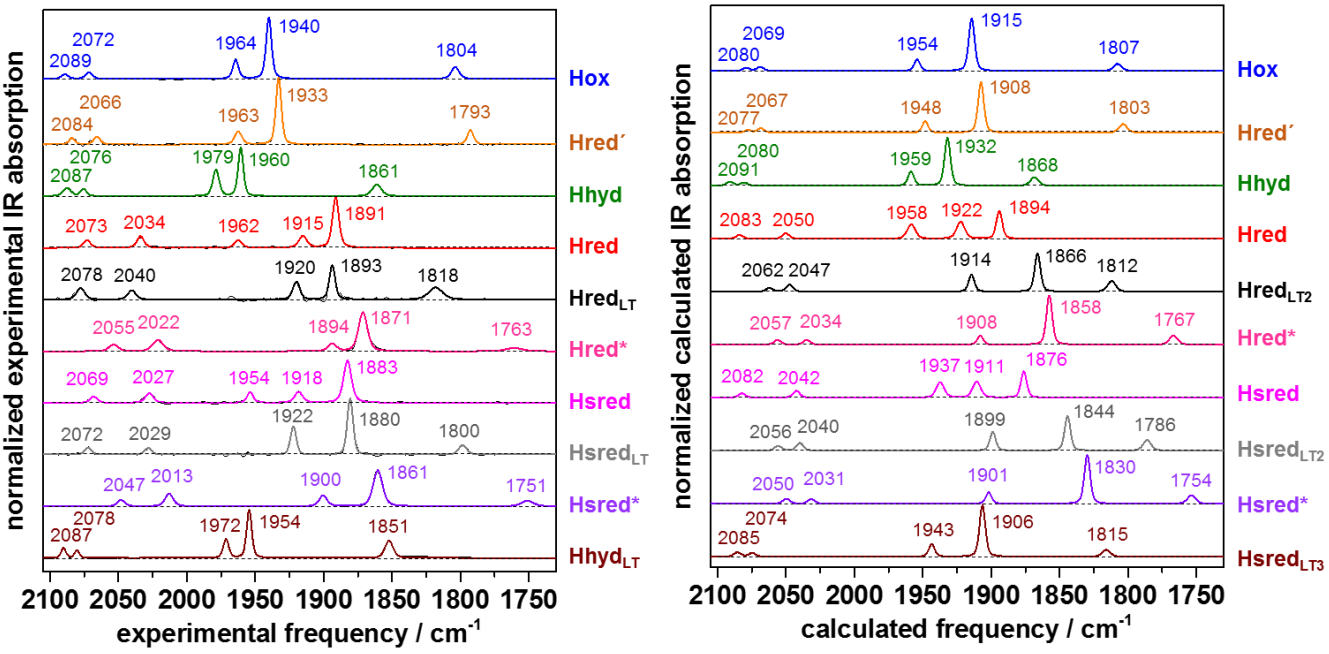

***Figure 3:*** *FTIR spectra of H-cluster states in CrHydA1 at ambient or cryogenic temperatures. Left panel: experimental spectra of pure H-cluster states (black lines) and fit curves with indicated frequencies (colored lines); no index, spectra obtained at room temperature; LT, spectra at cryogenic temperatures. The* ***Hox****,* ***Hred****, and* ***Hsred*** *spectra (298 K) correspond to our data in Fig. 2, the* ***Hred´*** *and* ***Hhyd*** *spectra were taken from our earlier reports,[11, 29] the* $\mathbf{Hred_{LT}}$ *and* $\mathbf{Hhyd_{LT}}$ *spectra (100 K) were derived from data in ref.[18] (see SI text), the* $\mathbf{Hsred_{LT}}$ *spectrum (4 K) was derived from data in ref.[17] (Figs. S4-S6 and Table S5). Spectra denoted* ***Hred**** *and* ***Hsred**** *were derived from room temperature data in ref.[24] for a sensory [FeFe]-hydrogenase (Fig. S8). Right panel: calculated spectra including the mean frequency values and band intensities (stick spectra broadened similar to the experimental spectra) from four quantum chemical computation procedures (see Fig. S10 for technical details and for standard deviations of the calculated IR band frequencies). Low-temperature models: LT2,* $\mu$*CO and additional proton at N(adt); LT3,* $\mu$*CO and apical hydride at* $Fe_d$*. A spectrum of a structure (LT1) with a semi-bridging CO and an additional proton at N(adt) is shown in Fig. S13. Spectra were vertically stacked for clarity.*

Recently, FTIR temperature series of reduced *Cr*HydA1 and *Dd*H were reported.[17] We analyzed the respective raw, room temperature FTIR spectra of *Cr*HydA1 (mainly **Hsred**) or *Dd*H (mainly **Hred**), including quantification of the temperature-dependent spectral changes (see SI text and Fig. S4 for details). As noted also in ref.[17], visual inspection of the spectra reveals an apparent increase of some band intensities in the $\mu$CO region and frequency shifts of the main bands of **Hred** and **Hsred**, as well as relative amplitude changes in the terminal CO regions, when decreasing the temperature from 280 K to 4 K (Fig. S4). We used a fit approach including various H-cluster states to analyze the temperature series and assumed the existence of each two species, which correspond to **Hred** and **Hsred** at room temperature (3 terminal CO ligands and lacking a low-frequency $\mu$CO band, Fig. 2), as well as to $\mathbf{Hred_{LT}}$ and $\mathbf{Hsred_{LT}}$ at cryogenic temperatures (2 terminal CO bands and showing a low-frequency $\mu$CO band, Fig. 2). All FTIR spectra could be well described by this approach (Figs. S4-S7, Table S5).

The following observations were made: ***(i)*** The total IR spectral intensities increased ca. 1.5-fold from about 280 K to 50 K and levelled off at lower temperatures. This effect is known from IR data of various systems[60-62] and is explained by the Einstein/Debye model of phonon-lattice interactions (see SI text).[63-64] Here, the effect bears the danger of visual overestimation, e.g., of the $\mu$CO band at cryogenic temperatures. Only normalized spectra allow for species quantification. ***(ii)*** There is no significant increase of the mean IR band widths or global shift of band frequencies when increasing the temperature. The broadening of $\mu$CO bands as proposed in ref.[17] is due to the neglect in the analysis of $\mu$CO contributions in the 1790-1810 $cm^{-1}$ region from other H-cluster states than **Hred$_{LT}$** and **Hsred$_{LT}$** such as **Hox-CO**, **Hred´**, and **Hred´-CO**. ***(iii)*** Non-quantitative populations of **Hred** and **Hsred** at 280 K (ca. 20-65 %), a fractional decrease of the latter species populations and increase of **Hred$_{LT}$** and **Hsred$_{LT}$** (to ca. 5-35 % at 4 K), as well as a population decrease of **Hred´** and **Hhyd** when lowering the temperature were found. ***(iv)*** The pure spectra of **Hred** in *Dd*H and **Hsred** in *Cr*HydA1 are very similar to our *Cr*HydA1 spectra in Fig. 2. Respective pure spectra including **Hred$_{LT}$** and **Hsred$_{LT}$** are shown in Figs. S5, S6, and Fig. 3. Pure spectra of **Hred$_{LT}$** and **Hhyd$_{LT}$** for *Cr*HydA1 were derived from FTIR data at 100 K in ref.[18] and are shown as well in Fig. 3. The IR spectra of **Hred$_{LT}$** and **Hsred$_{LT}$** reveal a $\mu$CO band and $\leq$5 $cm^{-1}$ shifts of the other CO and $CN^-$ bands relative to **Hred** and **Hsred** at room temperature. Similar band shifts for **Hred** vs. **Hred$_{LT}$** were reported in an earlier study on *Ca*I.[16] ***(v)*** The temperature dependence of the **Hred/Hred$_{LT}$** and **Hsred/Hsred$_{LT}$** population changes showed a steeper slope in the range of about 200-280 K than below ~200 K (Fig. S7). Such a "breakpoint" behavior is typically observed for parameters, such as, e.g., the crystallographic mean-square displacement of atoms, that follow the so-called "protein-glass transition".[38-40] Since the transition effect is attributed to the freezing-out of vibrations in the protein (see the XAS section), the increased low-temperature **Hred$_{LT}$** and **Hsred$_{LT}$** populations may be related to the restriction of certain molecular motions (Fig. S7).

Interestingly, FTIR spectra with similar signatures as **Hred$_{LT}$** and **Hsred$_{LT}$**, but showing overall about ~20 $cm^{-1}$ lower frequencies of the terminal $CN^-$/CO ligands and even ~50 $cm^{-1}$ lower $\mu$CO frequencies (1751 $cm^{-1}$, 1763 $cm^{-1}$), were assigned to **Hred*** and **Hsred*** states in a putative sensory [FeFe]-hydrogenase from *Thermotoga maritima* (Fig. S8, Table 1).[24] However, its **Hox** bands were quite similar to *Cr*HydA1 (Fig. S8).[24] According to our earlier results,[11, 20-21, 29-30, 65] we anticipate that the deviating CO/$CN^-$ frequencies in the various Hred-like species are related to different electron/proton distributions, as well as to different ligand configurations at the diiron site, which is investigated further below.

***X-ray absorption spectroscopy probing the protein-glass transition.*** *Cr*HydA1 solution samples prepared for XAS experiments showed mainly oxidized or reduced H-cluster states according to the FTIR reference spectra (Fig. S2). Quantitative analysis (Table S4) revealed that the CO band spectra of the samples were essentially described by five H-cluster states (**Hox**, **Hox-CO**, **Hred´**, **Hred**, **Hsred**) with varying populations (Fig. S3), prevalence of oxidized or reduced states to each about 65±5 % in the two sample types, and a minor contribution of unbound $2Fe_{adt}$, similar to the spectra in Fig. 2. XANES and EXAFS spectra at the Fe K-edge were collected on the *Cr*HydA1 samples in a temperature range of about 25 – 275 K. The XANES spectra of both sample types were very similar and similar to earlier reported spectra.[29, 65-67] Their shapes were practically temperature independent, the K-edge energies were constant (±0.05 eV), and the K-edge energy of the reduced enzyme was ~0.1 eV lower compared to the oxidized enzyme (Figs. 4 and S9). This result proved the absence of X-ray photo-reduction of the H-cluster, meaning a constant overall oxidation state of iron during XAS data collection in the whole temperature range, and further implied the absence of larger structure or redox changes in response to the temperature increase. We note that an overall similar oxidation state of iron in the *Cr*HydA1 samples was expected due to reduction and protonation at the H-cluster when mainly converting **Hox** into **Hred´** and **Hred** (Fig. S2).

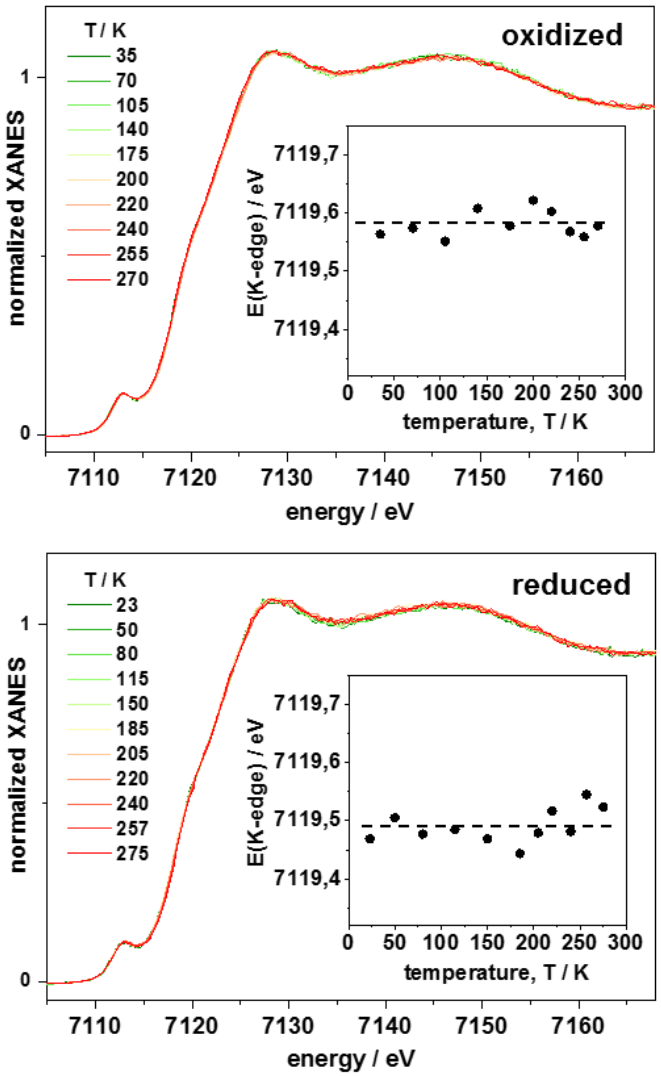


***Figure 4:*** *Temperature series of Fe XANES spectra of CrHydA1. Top panel: oxidized protein. Bottom panel: reduced protein. Spectra correspond to samples with prevailing (~65±5 %) oxidized (mainly* ***Hox****) or reduced (mainly* ***Hred´*** *and* ***Hred****) H-cluster states as derived from FTIR analysis (Fig. S2) and were collected at the indicated temperatures (±2 K). The insets show the K-edge energies (at about edge half-height, dashes mark the mean energies). Fig. S9 shows a direct comparison of mean spectra of oxidized or reduced CrHydA1.*

Temperature series of EXAFS spectra are shown together with the results of simulation analyses in Fig. 5. Visual inspection of the spectra of oxidized or reduced *Cr*HydA1 revealed similar shapes and changes in the temperature range, in particular featuring small decreases of the first main Fourier-transform (FT) peak due to Fe-C(=N/O) and Fe-S interactions and larger

decreases of the second main FT peak comprising major contributions from the Fe-Fe distances in $[2Fe]_H$ and $[4Fe]_H$ for increasing temperatures (Figs. 5A,B and S9).[67]

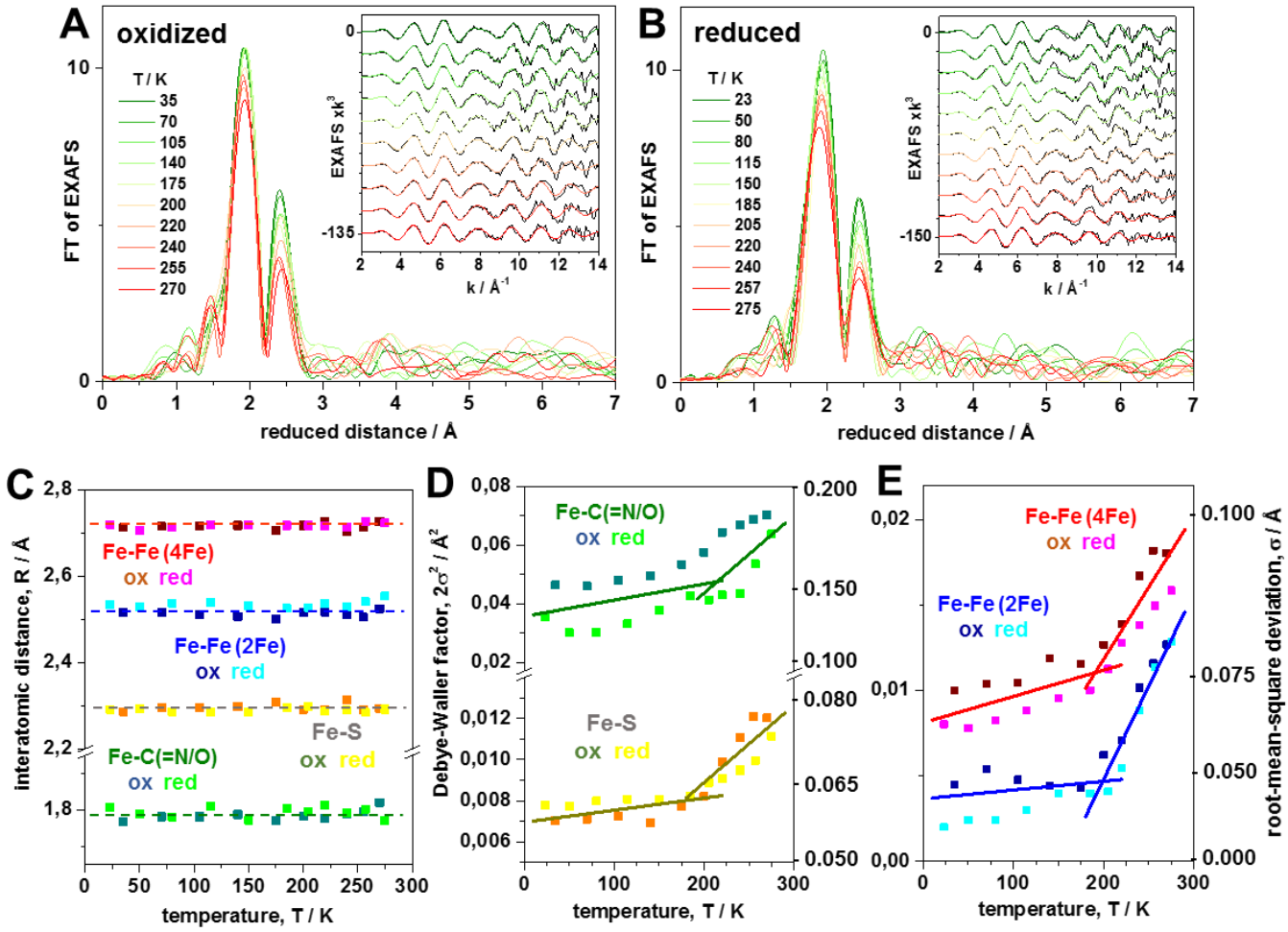


***Figure 5:*** *Temperature dependence of EXAFS spectra of CrHydA1. Data correspond to XANES and FTIR spectra in Figs. 4 and S2. (A) Fourier-transforms of EXAFS spectra in the inset of oxidized CrHydA1. (B) Fourier-transforms of EXAFS spectra in the inset of reduced CrHydA1. Main panels: experimental data; insets: black lines, experimental data and colored lines, simulations (vertically stacked). (C) Interatomic distances, R, from EXAFS simulations (dashed lines guide the eye). (D and E) Respective Debye-Waller factors, $2\sigma^2$ (left y-axes), for iron-ligand bonds (D) or Fe-Fe distances (E) (smoothed over 2 data points). Corresponding root-mean-square deviations, $\sigma$, of interatomic distances are shown on the right y-axes in panels D and E. The lines in (D and E) are linear fits for mean $2\sigma^2$ values of oxidized and reduced CrHydA1 below or above 200 K. The EXAFS fits comprised the following coordination numbers, N, per Fe ion (mean R values or values for ox/red ±standard deviation in parenthesis): Fe-C(=N/O) (2.29±0.01 Å) and Fe(-C)=N/O = 1 (R = 3.1±0.05 Å), Fe-S = 3.33*

*(2.30±0.01 Å / 2.29±0.01 Å), Fe-Fe (2Fe) = 0.33 (2.51±0.02 Å / 2.53±0.02 Å), Fe-Fe (4Fe) = 2 (2.72±0.02 Å), and a multiple-scattering contribution of the C=N/O ligands (N = 1, R = 0.80±0.03 Å, $2\sigma^2$ as for Fe-C=N/O). Fig. S9 compares mean spectra of oxidized or reduced CrHydA1 (simulation parameters in Table 2).*

**Table 2:** EXAFS simulation parameters.[a]

| shell | ox. | red. | ox. | red. | ox. | red. |
|---|---|---|---|---|---|---|
| | N [per Fe] | | R [Å] | | $2\sigma^2$ x$10^3$ [Å$^2$] ($\sigma$ [Å]) | |
| Fe-C(=N/O) | 0.38$^{\#}$ | 0.55$^{\#}$ | 1.77 (1.78) | 1.82 | 10$^{\&}$ (0.071) | 6$^{\&}$ (0.055) |
| Fe-C(=N/O) | 0.62$^{\#}$ | 0.45$^{\#}$ | 1.95 (1.91) | 2.07 | 10$^{\&}$ (0.071) | 6$^{\&}$ (0.055) |
| Fe-S | 3.17* | 3.17* | 2.28 (2.29) | 2.29 | 8 (0.063) | 8 (0.063) |
| Fe(-C)=N/O | 1* | 1* | 2.92 (2.97) | 2.90 | 10$^{\&}$ (0.071) | 6$^{\&}$ (0.055) |
| (Fe-C)=N/O$_{ms}$ | 1* | 1* | 1.22 (1.18) | 1.19 | 10$^{\&}$ (0.071) | 6$^{\&}$ (0.055) |
| Fe-Fe (2Fe) | 0.33* | 0.33* | 2.49 (2.55) | 2.52 | 2* (0.032) | 2* (0.032) |
| Fe-Fe (4Fe) | 2* | 2* | 2.70 (2.69) | 2.71 | 13 (0.081) | 15 (0.087) |

[a]Parameters correspond to simulations of mean EXAFS spectra over all temperatures of oxidized or reduced *Cr*HydA1 in Fig. S9B (inset). The error sum ($R_F$, deviation in % between experimental Fourier back-transform and calculated EXAFS spectrum for a reduced distance range of 1-3 Å) was 5.5 % (ox.) or 8.7 % (red.). *Fixed parameter, $^{\#}$N-values coupled to a sum of 1, $^{\&}2\sigma^2$ coupled to yield equal values, ms denotes a multiple-scattering contribution. R-values from a crystal structure (≥5 % error) of oxidized *Cp*I (**Hox**)[8] in parenthesis (Fig. 1).

EXAFS simulations revealed the following main structural features of the H-cluster in the two sample types: ***(i)*** The mean iron-ligand bond lengths and Fe-Fe distances were similar to earlier XAS results[29, 67] and well compatible with crystal structures (Table 2). Overall similar interatomic distances in the oxidized or reduced *Cr*HydA1 were expected due to the similar prevailing structural motifs in the dominant H-cluster states (i.e., **Hox** or **Hred´** with a $\mu$CO) in the XAS samples (Fig. S2). An overall elongation (~0.05 Å) of the Fe-C(=N/O) distances was accompanied by an about 1.5-fold decrease of the Debye-Waller factor, which is attributed to a homogenization of the Fe-C(=N/O) bond lengths due to the lack of a $\mu$CO in a significant

fraction (~35 % **Hred** and **Hsred** states) of the reduced *Cr*HydA1. ***(ii)*** The interatomic distances were temperature independent (i.e., constant within the fit error range of ±0.02 Å or less) (Fig. 5C). For a bond length change of only 0.01 Å, a frequency change of ~12 $cm^{-1}$ may be estimated for, i.e., the C=N/O stretching vibration (see SI text). Because such large frequency changes were not observed in the FTIR temperature series, the bond lengths are presumably constant on a less than 0.01 Å scale. ***(iii)*** The Debye-Waller parameters ($2\sigma^2$, $\sigma$ corresponds to the root-mean-square deviation of the absorber-backscatterer distance) of the iron-ligand bonds and in particular of the Fe-Fe distances were significantly increasing with increasing temperature and revealed apparent "breakpoint" behavior around 200 K as indicative of the protein-glass transition (Fig. 5D,E). The protein-glass transition behavior can be interpreted as resulting from harmonic iron-ligand bond vibrations that proceed in the whole temperature range, while larger-scale coupled molecular motions affecting the iron displacements, as identified for example in the <250 $cm^{-1}$ frequency range by $^{57}$Fe nuclear resonance (X-ray) vibrational spectroscopy (NRVS),[20, 29, 32, 68] proceed most effectively at ambient temperatures and may essentially be frozen out below ~200 K. Since the EXAFS may be expected to reflect mostly local interatomic distance disorder, the pronounced $2\sigma^2$ increase above ~200 K could further suggest a change in the relative H-cluster state populations and/or structures, e.g., formation of species with a by ≤0.03 Å increased mean Fe-Fe distance spread (but similar absolute mean Fe-Fe distances).

***H-cluster structure assignment.*** Quantum chemical calculations on H-cluster models were performed to derive geometry-optimized structures and the CO/$CN^-$ normal modes. We followed the routines established in our earlier studies, using four different approaches, i.e., BP86 pure or TPSSh hybrid functionals for DFT or QM/MM calculations on smaller or larger structures (Figs. S10, S15).[9, 20-21, 29] Normal mode analysis and broadening of stick spectra provided theoretical IR spectra for comparison with the experimental spectra (Fig. 3). As found earlier, the absolute IR frequencies and intensities varied (moderately) depending on the theory

level, but the trends of the spectral changes were generally highly conservative (see the caption of Fig. S10 for a more detailed account on systematic effects in the quantum chemical calculations). Overall, the frequency differences for the use of the different functionals were larger than for DFT vs. QM/MM models. The TPSSh or BP86 functionals yielded globally too high or too low IR frequencies so that the averaged frequencies were already quite close to the experimental values. The TPSSh functional further caused an underestimation of CO band down-shifts relative to the $CN^-$ bands upon reduction, which was reverse for the BP86 functional. Fundamental differences in the performance of the quantum chemical approaches for calculation of IR spectra of the H-cluster were not observed, in agreement with our earlier work. Accordingly, the calculated frequencies for each approach were corrected for systematic differences to the experimental data and the corrected frequencies and intensities were averaged (Fig. S10, giving also an apparent frequency standard deviation), thereby deriving mean IR spectra of the studied H-cluster states. In the following, we refer to the mean and corrected, calculated IR data, if not stated otherwise. The outlined approach yielded IR spectra of **Hox** and of 13 models for reduced H-cluster states at room temperature (**Hred´**, **Hhyd**, **Hred**, **Hred***, **Hsred**, **Hsred***) or low temperature (**Hred**$_{LT1,2,3}$, **Hsred**$_{LT1,2,3}$). The structures for the room temperature states reproduced most of the experimental spectral changes that were observed in comparison to the oxidized state, **Hox** (Fig. 3). A correlation plot of calculated vs. experimental IR frequencies accordingly shows good linearity ($R^2 = 0.97$) (Fig. S10). Also the frequency differences were well correlated. Furthermore, the root mean square deviation (rmsd) between calculated and experimental IR frequencies was small (ca. 10 – 15 $cm^{-1}$), indicating good agreement for the states that could be assigned with high certainty (Tables 3 and S6).

**Table 3:** H-cluster configurations and IR frequency correlation.

| H-cluster species | | $[4Fe]_H$ | $[2Fe]_H$ | $[2Fe]_H$ | H-species at: | | total | rmsd |
|---|---|---|---|---|---|---|---|---|
| experiment | calculation | state[a] | state[b] | $\mu$CO | $[4Fe]_H$ | $[2Fe]_H$ | charge | $[cm^{-1}]$[c] |
| **Hox** | **Hox** | 2+ | II,I | yes | – | – | -3 | 13.3 |
| **Hred´** | **Hred´** | + | II,I | yes | $H^+_{cys}$ | – | -3 | 12.5 |
| **Hhyd** | **Hhyd** | + | II,II | yes | $H^+_{cys}$ | $H^-_{Fed}$ | -3 | 14.1 |
| **Hred** | **Hred** | 2+ | II,II | no | – | $\mu H^-$ | -3 | 9.5 |
| **Hred$_{LT}$** | **Hred$_{LT2}$** | 2+ | I,I | yes | – | $H^+_{Nadt}$ | -3 | 11.5 |
| **Hred*** | **Hred*** | 2+ | I,I | yes | – | – | -4 | 10.6 |
| **Hsred** | **Hsred** | + | II,II | no | – | $\mu H^-$ | -4 | 12.6 |
| **Hsred$_{LT}$** | **Hsred$_{LT2}$** | + | I,I | yes | – | $H^+_{Nadt}$ | -4 | 21.9 |
| **Hsred*** | **Hsred*** | + | I,I | yes | – | – | -5 | 15.3 |
| **Hhyd$_{LT}$** | **Hsred$_{LT3}$** | + | II,II | yes | – | $H^-_{Fed}$ | -4 | 29.8 |

[a]$[4Fe]_H$ charges of 2+ or + correspond to formal $II_2III_2$ or $II_3III$ redox configurations. [b]Iron redox states ($Fe_p$,$Fe_d$) and the hydride charge represent formal assignments. [c]rmsd values are for mean calculated IR frequencies in Figs. 3 and S10C and were derived with Eq. S7 (Table S6 shows the complete correlation matrix). The experimentally observed low-temperature states **Hred$_{LT}$**, **Hsred$_{LT}$**, **Hhyd$_{LT}$** were termed **HredH$^+$**, **HsredH$^+$**, **Hhyd:red** in refs.[17-18] (see the Discussion).

The models for room temperature H-cluster states that correspond to the calculated IR spectra reveal the following main features and changes compared to **Hox** (Fig. 6): ***(i)*** A structure with a vacancy at $Fe_d$ as in crystals accounts for the IR spectrum of **Hox** and provides a crucial reference point for comparison of experimental and calculated data. ***(ii)*** The IR signatures of **Hred´** and **Hhyd** were well described by structures with a $\mu$CO and a proton at a cysteine sulfur of the $[4Fe]_H$ cluster (C499 in *Cp*I notation), further including a reduced $[4Fe]_H$ in **Hred´** or a reduced $[4Fe]_H$ and a terminal hydride ($H^-$) at $Fe_d$ of the reduced diiron site in **Hhyd**.[11, 29] There is broad consensus on the apical hydride in **Hhyd**.[12, 16-17, 26] ***(iii)*** The spectra of **Hred** and **Hsred** that lack a $\mu$CO band and show the largest CO band at lowest frequencies as well as an about 2.5-fold wider $CN^-$ frequency gap vs. **Hox** were best reproduced by $1e^-$ or $2e^-$ reduced structures with a bridging hydride ($\mu H^-$). Our earlier studies[20-21] and the present data (Figs. S11, S12; Table S6) show that structures without a $\mu$CO that carry a further proton at N(adt) do not agree

well with the IR (and NRVS[20]) spectra of **Hred/Hsred**. The $\mu H^-$ structures also agree with the lack of IR band shifts due to H/D exchange (Table S7). ***(iv)*** Models for **Hred*/Hsred*** that lack H-cluster protonation nicely yielded the large IR band down-shifts vs. **Hox** and the main frequency differences between the two states. The $CN^-$ frequency gap was underestimated, pointing to further structural changes at the diiron site, perhaps due to the altered amino acid environment in the sensory [FeFe]-hydrogenase.[24, 69]

IR spectra were calculated for three different model structures for the low-temperature H-cluster species (**Hred$_{LT}$**, **Hsred$_{LT}$**), which show **(1)** an unoccupied bridging site at $[2Fe]_H$ and an additional proton at N(adt), **(2)** a $\mu$CO and an additional proton at N(adt), or **(3)** a $\mu$CO and an apical hydride at $Fe_d$ (Figs. 6, S11-S3). The following observations were made: ***(i)*** The **Hred$_{LT1}$** and **Hsred$_{LT1}$** structures showed inverted CO band patterns lacking a $\mu$CO band, with the smallest instead of the largest CO band at intermediate frequencies, which is incompatible with the experimental data (Figs. 3, S11-S13), thus excluding such structures. ***(ii)*** The **Hred$_{LT2}$/Hsred$_{LT2}$** and **Hred$_{LT3}$/Hsred$_{LT3}$** models yielded IR band patterns with the largest CO band at intermediate frequencies and a low-frequency $\mu$CO band similar to the experimental data and further reproduced the main band shifts for **Hsred$_{LT}$** vs. **Hred$_{LT}$** (Figs. 3, S11-S13). Notably, **Hred$_{LT2}$** was a transient (saddle point) structure that mostly converted to **Hred$_{LT1}$** while the **Hsred$_{LT2}$** structure in some cases was a true (albeit shallow) energetic minimum. The rmsd was best for **Hred$_{LT2}$** and **Hsred$_{LT2}$** with a proton at N(adt) (Table 3). The more oxidized iron in $[2Fe]_H$ in the terminal-hydride structures resulted in overall higher IR frequencies vs. the N(adt)-protonation structures, so that the latter spectra showed most bands at lower frequencies than **Hox**, more similar to the experimental data. ***(iii)*** H/D exchange at the H-cluster gave downshifts of only the $\mu$CO band by >18 $cm^{-1}$ for the terminal-hydride structures, but no such shifts in the N(adt)-protonation structures (Table S7), in apparently better agreement with most experimental data (see the Discussion). ***(iv)*** The enlarged experimental $CN^-$ frequency

gap in **Hred**$_{LT}$/**Hsred**$_{LT}$ vs. **Hox** was not fully reproduced by the model structures, which may be attributed to further changes at the H-cluster site at low temperatures that cannot be considered reliably in the calculations. ***(v)*** After addition of a proton at N(adt) and one electron to the starting structure (**Hox**), movement of the initial $\mu$CO into a terminal position at Fe$_d$ was observed during geometry optimization so that the $\mu$CO structure converted to the open-bridge structure (see SI text and movie). The reason is that the non-bridging structures with a protonated N(adt) were stabilized by being at ~180 meV (**Hred**$_{LT1}$) or ~70 meV (**Hsred**$_{LT1}$) lower energies vs. the respective $\mu$CO structures (**Hred**$_{LT2}$, **Hsred**$_{LT2}$) (Table S8). Furthermore, the terminal-hydride structures were at more than -400 meV lower energies than both protonated N(adt) models (Table S8). The relative energies support that opening of the $\mu$CO bridge is favored at room temperature under conditions where N(adt) protonation is faster than [4Fe]$_H$ protonation so that $\mu$H$^-$ binding can occur to yield, i.e., **Hred**, while at low temperatures, $\mu$CO bridge opening and [4Fe]$_H$ protonation are prevented so that structures with an additional proton at N(adt) or perhaps a terminal hydride at Fe$_d$ are trapped.

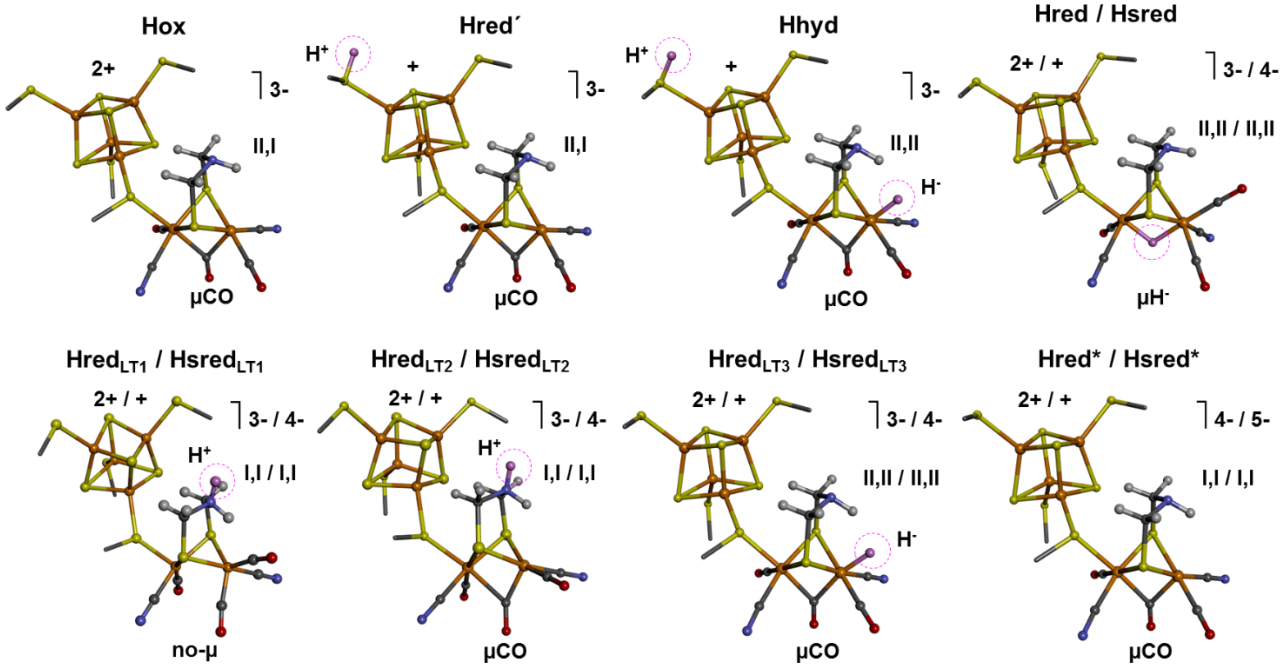

***Figure 6:*** *H-cluster model structures. LT, models for low-temperature H-cluster states (Fig. S12). The shown cofactor structures can account for IR spectra in Fig. 3 (except LT1 structures, often resulting from LT2 structures in the calculations, see SI movie for a typical conversion of a* $\mathbf{Hred}_{LT2}$ *to a* $\mathbf{Hred}_{LT1}$ *structure at BP86/DFT level).* $[4Fe]_H$ *charges, formal redox states of the diiron sub-complex, and total cofactor charges are indicated. Magenta circles mark protonation at Cys499 (CpI numbering), additional protonation at N(adt), or hydride (*$H^-$*) binding in bridging or terminal positions at* $[2Fe]_H$ *(no-*$\mu$*, open bridge position).*

## Discussion

Our results suggest that the so-far identified H-cluster states are dissected into two basic configurations with or without a $\mu$CO ligand. At ambient temperatures where [FeFe]-hydrogenases function, three $\mu$CO states can be accumulated (**Hox**, **Hred´**, **Hhyd**; Fig. 6). Our data consistently suggests that reduced **Hred´** and **Hhyd**, as well as oxidized **HoxH** contain a surplus proton at $[4Fe]_H$ (at Cys499).[11, 20, 29-30, 46] Assignment of $[4Fe]_H$ protonation was based on statistical comparison of experimental and computational FTIR and NRVS data[11, 20, 30] and is supported by the effects of mutations around the cubane cluster,[70] crystal data showing two orientations of a neighboring serine in oxidized or reduced *Cp*I,[36] and EPR results.[71] Further work (e.g., ENDOR) to clarify the $[4Fe]_H$ protonation state is, however, highly desirable. Integration of the above four states in a catalytic cycle is consistently rationalized as outlined in our earlier studies[11-13, 19, 72] and here is summarized in the SI text (see ref. 2 for a review) (Fig. 7). This catalytic cycle proposal is fully consistent also with our present analyses.

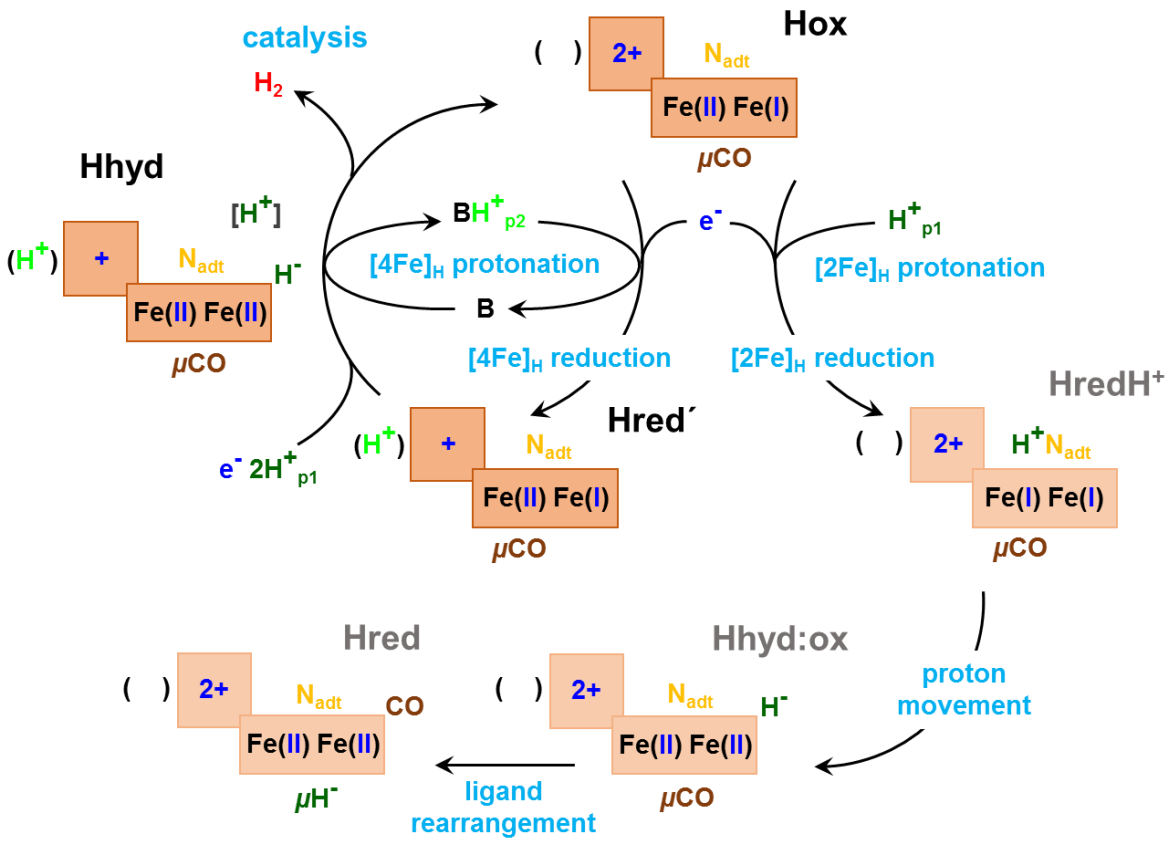


***Figure 7:*** *H-cluster reaction pathways. In the catalytic cycle starting from* ***Hox****, the first reduction and protonation via channel p2 from a base (B, possibly a water molecule) at a cysteine ligand of* $[4Fe]_H$ *yields* ***Hred´****, which after a second reduction and transfer of two protons via channel p1 including the N(adt) yields* $H_2$*. PCET and* $H_2$ *formation reactions after* ***Hred´*** *comprise* ***Hhyd*** *and possibly further transient species (e.g.,* ***HoxH****). Hindered* $[4Fe]_H$ *protonation via channel p2 biases the first reduction to* $[2Fe]_H$ *and, at room temperature, results in transient N(adt) (****HredH*****$^+$*) or* $Fe_d$ *(****Hhyd:ox****) protonation via channel p1, so that ligand rearrangement can yield a* $\mu H^-$ *in* ***Hred*** *as a state at lowest energy.* $[4Fe]_H$ *protonation and ligand rearrangement are proposed to be impaired at cryogenic temperatures. A further reduction gives the respective* ***HsredH*****$^+$***,* ***Hhyd:red****, and* ***Hsred*** *species (not shown). For details on the rationalization of our catalytic cycle proposal see SI text.*

At room temperature, two further reduced states become prominent preferentially at acidic pH where hydrogenase activity is low, which are 1e$^-$ (**Hred**) or 2e$^-$ (**Hsred**) reduced. Present data reinforce the view that a $\mu$CO is absent in these states. We assigned **Hred** and **Hsred** to

structures with a bridging hydride ($\mu H^-$), in agreement with the ~60 mV/pH Pourbaix slope due to a $1e^-/1H^+$ proton-coupled electron transfer (PCET) in the **Hox** → **Hred** transition.[19, 21] We emphasize that the $\mu H^-$ annotation corresponds to the formal assignment of the proton at the Fe-Fe bond to a hydride, i.e., as resulting from $1e^-$ oxidation of the iron ions and $2e^-$ reduction of the incoming proton due to $1e^-$ H-cluster reduction in **Hred**. Rather, earlier quantum chemical calculations showed that the actual (negative) charge on the proton is close to zero similar to **Hhyd**[29] and the iron centers of $[2Fe]_H$ are even slightly more reduced in **Hred** and **Hsred** (in comparison to **Hox**).[21] Accordingly, relatively small (overall) IR frequency (down-)shifts vs. **Hox** of the terminal (vibrationally coupled) CO ligands at $[2Fe]_H$ are expected in **Hred** and **Hsred**, as experimentally observed. With respect to $\mu$CO, our assignment of **Hred/Hsred** is supported by early crystal data of reduced *Dd*H, showing diminished electron density in the bridging position and ligand rearrangement at the diiron site.[23, 34] The crystal data has earlier been taken as an argument to propose a semi-bridging CO in **Hred/Hsred**, but now a $\mu$CO was anticipated.[17-19, 73] We propose that **Hred** formation is favored when protonation at $[2Fe]_H$ is more facile than protonation at $[4Fe]_H$. Protonation and reduction first at $[2Fe]_H$ induces $CN^-$/CO ligand rearrangement leading to $\mu H^-$ stabilization. Pronounced ligand rearrangement and $\mu H^-$ binding, i.e., resembling the $\mu H^-$ trap states of diiron site models,[74-76] seems incompatible with the large $H_2$ turnover rates of [FeFe]-hydrogenases.

In a putative sensory [FeFe]-hydrogenase, as well as in catalytic enzymes at cryogenic temperatures, further H-cluster states can be populated. **Hred*/Hsred*** were shown in the *Thermotoga maritima* protein HydS and attributed to $1e^-$ or $2e^-$ reduced, $\mu$CO species derived from **Hox** without H-cluster protonation.[24] Our results clearly support these assignments. Upon the first H-cluster reduction, the absence of protonation in the **Hox** → **Hred*** transition in HydS (as opposed to a protonation in the **Hox** → **Hred´/Hred** transitions in, e.g., *Cr*HydA1) is further seen by the much larger redox potential difference (ca. -270 mV vs. -60 mV at pH 8) and more

negative absolute potential (ca. -570 mV vs. -460 mV) of the second reduction step.[24, 33, 77] This finding nicely supports redox potential leveling due to the first PCET in the catalytic enzymes, thereby facilitating two sequential reductions at similar potentials as required by the $1e^-$ donors to the H-cluster (Fe-S clusters in bacterial enzymes or soluble ferredoxin PetF in *Cr*HydA1).

Recent reports suggested specific H-cluster states at cryogenic conditions (**Hred$_{LT}$/Hsred$_{LT}$**).[16-18] We support that the latter species correspond to structures with a bridging $\mu$CO as in **Hred´/Hhyd** (as opposed to a semi– or non-bridging CO). Two types of structures, with an additional proton at N(adt) or an apical hydride ($aH^-$) at $Fe_d$ and lacking $[4Fe]_H$ protonation may account for the IR signatures of **Hred$_{LT}$/Hsred$_{LT}$**. A thorough consideration (see SI text for a detailed discussion) of the available experimental and computational H/D-exchange IR and NRVS data and further results on the low-temperature states as well as on **Hred/Hsred** and **Hhyd**,[20-21, 27, 29, 32, 78-81] and of data for different [FeFe]-hydrogenases,[16-18] suggests that low-temperature species may even differ among the *Ca*I, *Cp*I, and HydA1 enzymes and, in summary, supports that reduced structures with additional N(adt) protonation predominantly accumulate at low temperatures. The proton at N(adt) may instead be bound as a hydride at $Fe_d$ in protein fractions under certain conditions, in particular in the $2e^-$ reduced state. Further structure changes at or close to the H-cluster at low temperatures may not be excluded. In an attempt to unify the nomenclature of H-cluster states, we suggest distinguishing low-temperature (i.e., **Hred$_{LT2}$/Hsred$_{LT2}$**) from room-temperature states by using **HredH$^+$/HsredH$^+$** for the former and **Hred/Hsred** for the latter (Fig. 7). $[2Fe]_H$ oxidized states with a reduced $[4Fe]_H$ should be referred to as **Hred´** (and **Hred´-CO**).

Our analyses suggest that **HredH$^+$/HsredH$^+$** form mostly at the expense of **Hred´/Hhyd** and **Hred/Hsred** during temperature lowering, showing typical "protein-glass transition" behaviour.[38-40] The EXAFS Debye-Waller parameter, corresponding to the mean square displacement of atoms in crystal structures,[82-83] reveals a clear "breakpoint" at ~200 K for the

oxidized and the reduced H-cluster. A similar glass-transition behavior observed before for metal cofactors in other proteins was often accompanied by vanishing activity.[84-88] We note that the absolute σ-values of the iron-ligand bonds or Fe-Fe distances of the H-cluster at cryogenic or ambient temperatures (about 0.04-0.10 Å) are well in the range or even at the lower limit of atomic displacements for other (metal) cofactors in enzymes.[38, 84-91] In brief, the common explanation for the protein-glass transition is that larger-scale anharmonic molecular motions, involving, e.g., amino acid side chain and hydrogen-bonded network rearrangements, are frozen out below the breakpoint. This can be due to protein mobility restrictions in response to a phase transition of water layers or clusters.[38-40, 83, 92] As such rearrangements, in particular involving water molecules and protonable sidechains in the protein interior, are essential for proton conduction along hydrogen-bonded pathways,[12, 93-94] the freezing-out of PCET reactions is expected below the transition temperature. Here, it seems that primarily those H-cluster states are diminished that carry a proton at $[4Fe]_H$ (**Hred´**, **Hhyd**) or bind a $\mu H^-$ (**Hred**, **Hsred**). We therefore suggest that proton transfer via the pathway to the $[4Fe]_H$ cluster becomes hindered at decreasing temperatures so that the first electron is biased not to the cubane, but to the diiron site. However, since ligand rearrangement at $[2Fe]_H$ for $\mu H^-$ binding also is impaired while proton transfer to the dithiolate is feasible, the proton ends up on the N(adt) (**HredH$^+$/HsredH$^+$**) (Fig. 7). As a note of caution, we state that whether the latter cofactor species represent intermediates or reflect a proton delivery pathway to the active site in the catalytic cycle, cannot be fully unambiguously defined at present, but such functions are not vitally required in our scheme (Fig. 7). Support for hindered low-temperature $[4Fe]_H$ protonation comes from strongly different EPR signals of the $[4Fe]_H^+$ sub-complex in **Hhyd** vs. **HsredH$^+$**.[18]

Interestingly, **HsredH$^+$** could be converted by ~100 K near-UV illumination to a state (**Hhyd:red**) attributed to a $2e^-$ reduced structure with an apical hydride at $Fe_d$ and lacking $[4Fe]_H$ protonation in contrast to **Hhyd**.[18] The additional proton at N(adt) in **HsredH$^+$** may

move to $Fe_d$ in **Hhyd:red**[18] and a similar situation may hold for the **HredH$^+$** to **Hhyd:ox** conversion (Fig. 7). Our calculations show that proton movement from N(adt) to $Fe_d$, but also protonation at $[4Fe]_H$ to form a low-temperature (i.e., **Hhyd$_{LT}$**) state from a structure with a proton already at $Fe_d$ can explain the light-induced IR differences[18] (Figs. 6, S14; Tables 3, S6). The more similar EPR power saturation in **Hhyd:red** and **Hhyd** vs. **HsredH$^+$**[18] may support a hydride before illumination. However, dissimilar structures may result at low (**Hhyd:red**) or ambient (**Hhyd)** temperatures, for example due to different protonation sites and/or altered cofactor/protein relaxation upon charge redistribution in response to protonation. Noteworthy, the reasons for any light-induced proton movement at the H-cluster are unclear at present.

H-cluster conversions raise the question on the relevance of [FeFe]-hydrogenase data collected at low temperatures. A detailed consideration (see SI text) suggests, e.g., inconsistencies in reduced state assignments, co-existence at least of **Hhyd**, **HredH$^+$/HsredH$^+$**, and **Hred/Hsred** down to 4 K, and observation of the relevant **Hox** structure in the crystals. We have earlier assigned NRVS data of HydA1 collected at ~50 K to **Hred** with a $\mu H^-$ in a sub-stoichiometric enzyme population, bearing the possibility for limited contributions from (reduced) $\mu$CO binding species under the respective conditions.[20] The present XAS data show that the H-cluster metrics remain practically constant in a 20-275 K range for *Cr*HydA1, meaning that significant structure changes do not occur. However, the precise state accumulations during temperature changes seem to depend on the specific enzyme as well as on the experimental procedures. The H-cluster species observed at cryogenic temperatures have been included in suggestions for the catalytic cycle of [FeFe]-hydrogenases. **HredH$^+$/HsredH$^+$** were represented as diiron site reduced states showing either a semi-bridging CO or a $\mu$CO[16, 18] at $[2Fe]_H$, as well as either two protons or one proton at N(adt),[16-18] while states with an apical hydride at $Fe_d$ were assumed to occur after Hsred-like species and to carry, e.g., a further proton at N(adt) or $[4Fe]_H$.[16-18, 29] Our results support a $\mu$CO in **HredH$^+$/HsredH$^+$** so that a semi-bridging CO can be excluded.

We agree with most other authors in the view that only $\mu$CO species should support fast catalysis. However, in our opinion there is no convincing argument that mandates inclusion of the low-temperature states in the catalytic cycle. These states seem to accumulate when protonation at $[4Fe]_H$ as well as ligand rearrangement and hydride binding at the diiron site are frozen out (Fig. 7). However, the apparent trapping of a proton at the N(adt) underpins the crucial importance of the dithiolate headgroup for proton conduction to the diiron active site.[12, 77, 95-96] Under functional conditions, dithiolate protonation states likely decay rapidly to the terminal hydride species, which provide the basis for most efficient $H_2$ formation chemistry.

**Acknowledgements**

Financial support by the Deutsche Forschungsgemeinschaft (to STS, contract no. STR1554/5-1; to MH, within UniSysCat, Cluster of Excellence Berlin, EXC1060) is gratefully acknowledged. We thank the beamline team (I. Zizak, G. Schuck) at KMC-3 of BESSY-II (Helmholtz Center Berlin) for technical support. We are indebted to the teams of T. Happe and U.-P. Apfel (Ruhr-Universität Bochum) for generously providing the $2Fe_{adt}$ reconstituted *Cr*HydA1 protein.

**Supporting Information available:**

Experimental and computational FTIR procedures (text), evaluation of infrared spectra (Figs. S1-S8, Tables S1-S5, separate spectra file), further XAS data (Fig. S9), computational data (Figs. S10-S14, Tables S6-S8, separate movie file), calculated H-cluster structures (Fig. S15, separate coordinates file).

## References


1. Lubitz, W.; Ogata, H.; Rudiger, O.; Reijerse, E., Hydrogenases. *Chem Rev.* **2014**, *114*, 4081-148.

2. Haumann, M.; Stripp, S. T., The molecular proceedings of biological hydrogen turnover. *Accounts Chem Res.* **2018**, *51*, 1755-1763.

3. Fontecilla-Camps, J. C.; Volbeda, A.; Cavazza, C.; Nicolet, Y., Structure/function relationships of [nife]- and [fefe]-hydrogenases. *Chemical Reviews.* **2007**, *107*, 4273-4303.

4. Mulder, D. W.; Shepard, E. M.; Meuser, J. E.; Joshi, N.; King, P. W.; Posewitz, M. C.; Broderick, J. B.; Peters, J. W., Insights into [fefe]-hydrogenase structure, mechanism, and maturation. *Structure.* **2011**, *19*, 1038-1052.

5. Land, H.; Senger, M.; Bergren, G.; Stripp, S. T., Current state of [fefe]-hydrogenase research: Biodiversity and spectroscopic investigations. *ACS catal.* **2020**, *10*, 7069–7086.

6. Nicolet, Y.; Piras, C.; Legrand, P.; Hatchikian, C. E.; Fontecilla-Camps, J. C., Desulfovibrio desulfuricans iron hydrogenase: The structure shows unusual coordination to an active site fe binuclear center. *Structure.* **1999**, *7*, 13-23.

7. Peters, J. W.; Lanzilotta, W. N.; Lemon, B. J.; Seefeldt, L. C., X-ray crystal structure of the fe-only hydrogenase (cpl) from clostridium pasteurianum to 1.8 angstrom resolution. *Science.* **1998**, *282*, 1853-1858.

8. Esselborn, J.; Muraki, N.; Klein, K.; Engelbrecht, V.; Metzler-Nolte, N.; Apfel, U. P.; Hofmann, E.; Kurisu, G.; Happe, T., A structural view of synthetic cofactor integration into [fefe]-hydrogenases. *Chem Sci.* **2016**, *7*, 959-968.

9. Senger, M.; Mebs, S.; Duan, J.; Wittkamp, F.; Apfel, U. P.; Heberle, J.; Haumann, M.; Stripp, S. T., Stepwise isotope editing of [fefe]-hydrogenases exposes cofactor dynamics. *P Natl Acad Sci USA.* **2016**, *113*, 8454-8459.

10. Silakov, A.; Wenk, B.; Reijerse, E.; Lubitz, W., N-14 hyscore investigation of the h-cluster of [fefe] hydrogenase: Evidence for a nitrogen in the dithiol bridge. *Phys Chem Chem Phys.* **2009**, *11*, 6592-6599.

11. Senger, M.; Mebs, S.; Duan, J. F.; Shulenina, O.; Laun, K.; Kertess, L.; Wittkamp, F.; Apfel, U. P.; Happe, T.; Winkler, M.; Haumann, M.; Stripp, S. T., Protonation/reduction dynamics at the [4fe-4s] cluster of the hydrogen-forming cofactor in [fefe]-hydrogenases. *Phys Chem Chem Phys.* **2018**, *20*, 3128-3140.

12. Duan, J. F.; Senger, M.; Esselborn, J.; Engelbrecht, V.; Wittkamp, F.; Apfel, U. P.; Hofmann, E.; Stripp, S. T.; Happe, T.; Winkler, M., Crystallographic and spectroscopic assignment of the proton transfer pathway in [fefe]-hydrogenases. *Nat Commun.* **2018**, *9*.

13. Senger, M.; Eichmann, V.; Laun, K.; Duan, J. F.; Wittkamp, F.; Knor, G.; Apfel, U. P.; Happe, T.; Winkler, M.; Heberle, J.; Stripp, S. T., How [fefe]-hydrogenase facilitates bidirectional proton transfer. *J Am Chem Soc.* **2019**, *141*, 17394-17403.

14. Albracht, S. P. J.; Roseboom, W.; Hatchikian, E. C., The active site of the [fefe]-hydrogenase from desulfovibrio desulfuricans. 1. Light sensitivity and magnetic hyperfine

interactions as observed by electron paramagnetic resonance. *Journal of Biological Inorganic Chemistry.* **2006**, *11*, 88-101.

15. Roseboom, W.; De Lacey, A. L.; Fernandez, V. M.; Hatchikian, E. C.; Albracht, S. P. J., The active site of the [fefe]-hydrogenase from desulfovibrio desulfuricans. Ii. Redox properties, light sensitivity and co-ligand exchange as observed by infrared spectroscopy. *Journal of Biological Inorganic Chemistry.* **2006**, *11*, 102-118.

16. Ratzloff, M. W.; Artz, J. H.; Mulder, D. W.; Collins, R. T.; Furtak, T. E.; King, P. W., Co-bridged h-cluster intermediates in the catalytic mechanism of [fefe]-hydrogenase cai. *J Am Chem Soc.* **2018**, *140*, 7623-7628.

17. Birrell, J. A.; Pelmenschikov, V.; Mishra, N.; Wang, H.; Yoda, Y.; Tamasaku, K.; Rauchfuss, T. B.; Cramer, S. P.; Lubitz, W.; DeBeer, S., Spectroscopic and computational evidence that [fefe] hydrogenases operate exclusively with co-bridged intermediates. *J Am Chem Soc.* **2020**, *142*, 222-232.

18. Lorent, C.; Katz, S.; Duan, J. F.; Kulka, C. J.; Caserta, G.; Teutloff, C.; Yadav, S.; Apfel, U. P.; Winkler, M.; Happe, T.; Horch, M.; Zebger, I., Shedding light on proton and electron dynamics in [fefe] hydrogenases. *J Am Chem Soc.* **2020**, *142*, 5493-5497.

19. Sommer, C.; Adamska-Venkatesh, A.; Pawlak, K.; Birrell, J. A.; Rudiger, O.; Reijerse, E. J.; Lubitz, W., Proton coupled electronic rearrangement within the h-cluster as an essential step in the catalytic cycle of [fefe] hydrogenases. *J Am Chem Soc.* **2017**, *139*, 1440-1443.

20. Mebs, S.; Duan, J. F.; Wittkamp, F.; Stripp, S. T.; Happe, T.; Apfel, U. P.; Winkler, M.; Haumann, M., Differential protonation at the catalytic six-iron cofactor of [fefe]-hydrogenases revealed by fe-57 nuclear resonance x-ray scattering and quantum mechanics/molecular mechanics analyses. *Inorg Chem.* **2019**, *58*, 4000-4013.

21. Mebs, S.; Senger, M.; Duan, J. F.; Wittkamp, F.; Apfel, U. P.; Happe, T.; Winkler, M.; Stripp, S. T.; Haumann, M., Bridging hydride at reduced h-cluster species in [fefe]-hydrogenases revealed by infrared spectroscopy, isotope editing, and quantum chemistry. *J Am Chem Soc.* **2017**, *139*, 12157-12160.

22. Rodriguez-Macia, P.; Pawlak, K.; Rudiger, O.; Reijerse, E. J.; Lubitz, W.; Birrell, J. A., Intercluster redox coupling influences protonation at the h-cluster in [fefe] hydrogenases. *J Am Chem Soc.* **2017**, *139*, 15122-15134.

23. Nicolet, Y.; de Lacey, A. L.; Vernede, X.; Fernandez, V. M.; Hatchikian, E. C.; Fontecilla-Camps, J. C., Crystallographic and ftir spectroscopic evidence of changes in fe coordination upon reduction of the active site of the fe-only hydrogenase from desulfovibrio desulfuricans. *J Am Chem Soc.* **2001**, *123*, 1596-1601.

24. Chongdar, N.; Birrell, J. A.; Pawlak, K.; Sommer, C.; Reijerse, E. J.; Rudiger, O.; Lubitz, W.; Ogata, H., Unique spectroscopic properties of the h-cluster in a putative sensory [fefe] hydrogenase. *J Am Chem Soc.* **2018**, *140*, 1057-1068.

25. Adamska, A.; Silakov, A.; Lambertz, C.; Rudiger, O.; Happe, T.; Reijerse, E.; Lubitz, W., Identification and characterization of the "super-reduced" state of the h-cluster in [fefe] hydrogenase: A new building block for the catalytic cycle? *Angew Chem Int Edit.* **2012**, *51*, 11458-11462.

26. Mulder, D. W.; Guo, Y. S.; Ratzloff, M. W.; King, P. W., Identification of a catalytic iron-hydride at the h-cluster of [fefe]-hydrogenase. *J Am Chem Soc.* **2017**, *139*, 83-86.

27. Winkler, M.; Senger, M.; Duan, J. F.; Esselborn, J.; Wittkamp, F.; Hofmann, E.; Apfel, U. P.; Stripp, S. T.; Happe, T., Accumulating the hydride state in the catalytic cycle of [fefe]-hydrogenases. *Nat Commun.* **2017**, *8*.

28. Gutierrez-Sanz, O.; Rudiger, O.; De Lacey, A. L., Ftir spectroscopy of metalloproteins. *Methods Mol Biol.* **2014**, *1122*, 95-106.

29. Mebs, S.; Kositzki, R.; Duan, J.; Kertess, L.; Senger, M.; Wittkamp, F.; Apfel, U. P.; Happe, T.; Stripp, S. T.; Winkler, M.; Haumann, M., Hydrogen and oxygen trapping at the h-cluster of [fefe]-hydrogenase revealed by site-selective spectroscopy and qm/mm calculations. *Biochim Biophys Acta Bioenerg.* **2018**, *1859*, 28-41.

30. Senger, M.; Laun, K.; Wittkamp, F.; Duan, J. F.; Haumann, M.; Happe, T.; Winkler, M.; Apfel, U. P.; Stripp, S. T., Proton-coupled reduction of the catalytic [4fe-4s] cluster in [fefe]-hydrogenases. *Angew Chem Int Edit.* **2017**, *56*, 16503-16506.

31. Fourmond, V.; Greco, C.; Sybirna, K.; Baffert, C.; Wang, P. H.; Ezanno, P.; Montefiori, M.; Bruschi, M.; Meynial-Salles, I.; Soucaille, P.; Blumberger, J.; Bottin, H.; De Gioia, L.; Leger, C., The oxidative inactivation of fefe hydrogenase reveals the flexibility of the h-cluster. *Nat Chem.* **2014**, *6*, 336-342.

32. Reijerse, E. J.; Pham, C. C.; Pelmenschikov, V.; Gilbert-Wilson, R.; Adamska-Venkatesh, A.; Siebel, J. F.; Gee, L. B.; Yoda, Y.; Tamasaku, K.; Lubitz, W.; Rauchfuss, T. B.; Cramer, S. P., Direct observation of an iron-bound terminal hydride in [fefe]-hydrogenase by nuclear resonance vibrational spectroscopy. *J Am Chem Soc.* **2017**, *139*, 4306-4309.

33. Silakov, A.; Kamp, C.; Reijerse, E.; Happe, T.; Lubitz, W., Spectroelectrochemical characterization of the active site of the [fefe] hydrogenase hyda1 from chlamydomonas reinhardtii. *Biochemistry-Us.* **2009**, *48*, 7780-7786.

34. Nicolet, Y.; Vernede, X.; Hatchikian, C. E.; Fontecilla-Camps, J. C., Structure of the reduced form of the iron-only hydrogenase from desulfovibrio desulfuricans atcc 7757. *Acta Crystallogr A.* **2000**, *56*, S94-S94.

35. Chernev, P.; Lambertz, C.; Brunje, A.; Leidel, N.; Sigfridsson, K. G. V.; Kositzki, R.; Hsieh, C. H.; Yao, S. L.; Schiwon, R.; Driess, M.; Limberg, C.; Happe, T.; Haumann, M., Hydride binding to the active site of [fefe]-hydrogenase. *Inorg Chem.* **2014**, *53*, 12164-12177.

36. Artz, J. H.; Zadvornyy, O. A.; Mulder, D. W.; Keable, S. M.; Cohen, A. E.; Ratzloff, M. W.; Williams, S. G.; Ginovska, B.; Kumar, N.; Song, J.; McPhillips, S. E.; Davidson, C. M.; Lyubimov, A. Y.; Pence, N.; Schut, G. J.; Jones, A. K.; Soltis, S. M.; Adams, M. W. W.; Raugei, S.; King, P. W.; Peters, J. W., Tuning catalytic bias of hydrogen gas producing hydrogenases. *J Am Chem Soc.* **2020**, *142*, 1227-1235.

37. Rodriguez-Macia, P.; Reijerse, E. J.; van Gastel, M.; DeBeer, S.; Lubitz, W.; Rudiger, O.; Birrell, J. A., Sulfide protects [fefe] hydrogenases from o2. *J Am Chem Soc.* **2018**, *140*, 9346-9350.

38. Doster, W., The protein-solvent glass transition. *Bba-Proteins Proteom.* **2010**, *1804*, 3-14.

39. Ringe, D.; Petsko, G. A., The 'glass transition' in protein dynamics: What it is, why it occurs, and how to exploit it. *Biophys Chem.* **2003**, *105*, 667-680.

40. Angell, C. A., The old problems of glass and the glass-transition, and the many new twists. *P Natl Acad Sci USA.* **1995**, *92*, 6675-6682.

41. Noth, J.; Esselborn, J.; Guldenhaupt, J.; Brunje, A.; Sawyer, A.; Apfel, U. P.; Gerwert, K.; Hofmann, E.; Winkler, M.; Happe, T., [fefe]-hydrogenase with chalcogenide substitutions at the h-cluster maintains full h-2 evolution activity. *Angew Chem Int Edit.* **2016**, *55*, 8396-8400.

42. Lampret, O.; Esselborn, J.; Haas, R.; Rutz, A.; Booth, R. L.; Kertess, L.; Wittkamp, F.; Megarity, C. F.; Armstrong, F. A.; Winkler, M.; Happe, T., The final steps of [fefe]-hydrogenase maturation. *P Natl Acad Sci USA.* **2019**, *116*, 15802-15810.

43. Esselborn, J.; Lambertz, C.; Adamska-Venkates, A.; Simmons, T.; Berggren, G.; Noth, J.; Siebel, J.; Hemschemeier, A.; Artero, V.; Reijerse, E.; Fontecave, M.; Lubitz, W.; Happe, T., Spontaneous activation of [fefe]-hydrogenases by an inorganic [2fe] active site mimic. *Nat Chem Biol.* **2013**, *9*, 607-609.

44. Esselborn, J.; Lambertz, C.; Adamska-Venkatesh, A.; Simmons', T.; Berggren, G.; Nothl, J.; Siebel, J.; Hemschemeier, A.; Artero, V.; Reijerse, E.; Fontecave, M.; Lubitz, W.; Happe, T., Spontaneous activation of [fefe]-hydrogenases by an inorganic [2fe] active site mimic. *Nature Chemical Biology.* **2013**, *9*, 607-609.

45. Berggren, G.; Adamska, A.; Lambertz, C.; Simmons, T. R.; Esselborn, J.; Atta, M.; Gambarelli, S.; Mouesca, J. M.; Reijerse, E.; Lubitz, W.; Happe, T.; Artero, V.; Fontecave, M., Biomimetic assembly and activation of [fefe]-hydrogenases. *Nature.* **2013**, *499*, 66-69.

46. Laun, K.; Mebs, S.; Duan, J.; Wittkamp, F.; Apfel, U. P.; Happe, T.; Winkler, M.; Haumann, M.; Stripp, S. T., Spectroscopical investigations on the redox chemistry of [fefe]-hydrogenases in the presence of carbon monoxide. *Molecules.* **2018**, *23*.

47. Schuth, N.; Mebs, S.; Huwald, D.; Wrzolek, P.; Schwalbe, M.; Hemschemeier, A.; Haumann, M., Effective intermediate-spin iron in o-2-transporting heme proteins. *P Natl Acad Sci USA.* **2017**, *114*, 8556-8561.

48. Kositzki, R.; Mebs, S.; Marx, J.; Griese, J. J.; Schuth, N.; Hogbom, M.; Schuemann, V.; Haumann, M., Protonation state of mnfe and fefe cofactors in a ligand-binding oxidase revealed by x-ray absorption, emission, and vibrational spectroscopy and qm/mm calculations. *Inorg Chem.* **2016**, *55*, 9869-9885.

49. Kass, D.; Corona, T.; Warm, K.; Braun-Cula, B.; Kuhlmann, U.; Bill, E.; Mebs, S.; Swart, M.; Dau, H.; Haumann, M.; Hildebrandt, P.; Ray, K., Stoichiometric formation of an oxoiron(iv) complex by a soluble methane monooxygenase type activation of o2 at an iron(ii)-cyclam center. *J Am Chem Soc.* **2020**, *142*, 5924-5928.

50. Dau, H.; Liebisch, P.; Haumann, M., X-ray absorption spectroscopy to analyze nuclear geometry and electronic structure of biological metal centers - potential and questions examined with special focus on the tetra-nuclear manganese complex of oxygenic photosynthesis. *Anal Bioanal Chem.* **2003**, *376*, 562-583.

51. Jorissen, K.; Rehr, J. J., New developments in feff: Feff9 and jfeff. *15th International Conference on X-Ray Absorption Fine Structure (Xafs15).* **2013**, *430*.

52. Rehr, J. J.; Kas, J. J.; Vila, F. D.; Prange, M. P.; Jorissen, K., Parameter-free calculations of x-ray spectra with feff9. *Phys Chem Chem Phys.* **2010**, *12*, 5503-5513.

53. Dapprich, S.; Komaromi, I.; Byun, K. S.; Morokuma, K.; Frisch, M. J., A new oniom implementation in gaussian98. Part i. The calculation of energies, gradients, vibrational frequencies and electric field derivatives. *J Mol Struc-Theochem.* **1999**, *461*, 1-21.

54. Vreven, T.; Morokuma, K., Hybrid methods: Oniom(qm:Mm) and qm/mm. *Ann Rep Comp Chem.* **2006**, *2*, 35-51.

55. al., M. J. F. e., Gaussian 09. *Gaussian, Inc., Wallingford CT.* **2016**.

56. Tao, J. M.; Perdew, J. P.; Staroverov, V. N.; Scuseria, G. E., Climbing the density functional ladder: Nonempirical meta-generalized gradient approximation designed for molecules and solids. *Phys Rev Lett.* **2003**, *91*.

57. Becke, A. D., Density-functional exchange-energy approximation with correct asymptotic-behavior. *Phys Rev A.* **1988**, *38*, 3098-3100.

58. Schafer, A.; Huber, C.; Ahlrichs, R., Fully optimized contracted gaussian-basis sets of triple zeta valence quality for atoms li to kr. *J Chem Phys.* **1994**, *100*, 5829-5835.

59. Rodriguez-Macia, P.; Reijerse, E.; Lubitz, W.; Birrell, J. A.; Rudiger, O., Spectroscopic evidence of reversible disassembly of the [fefe] hydrogenase active site. *J Phys Chem Lett.* **2017**, *8*, 3834-3839.

60. Zhang, M.; Salje, E. K. H.; Carpenter, M. A.; Wang, J. Y.; Groat, L. A.; Lager, G. A.; Wang, L.; Beran, A.; Bismayer, U., Temperature dependence of ir absorption of hydrous/hydroxyl species in minerals and synthetic materials. *Am Mineral.* **2007**, *92*, 1502-1517.

61. Chase, B.; Herron, N.; Holler, E., Vibrational spectroscopy of c-60 and c-70 temperature-dependent studies. *J Phys Chem-Us.* **1992**, *96*, 4262-4266.

62. Wang, W. F.; Stevenson, A.; Reuter, D. C.; Sirota, J. M., Absolute band intensities of acetone ((ch3)(2)co) in the infrared region of 830-3200 cm(-1) at low and room temperatures. *Spectrochim Acta A.* **2001**, *57*, 1603-1610.

63. Illinger, K. H.; Freeman, D. E., Temperature dependence of infrared and raman intensities. *J Mol Spectrosc.* **1962**, *9*, 191-&.

64. Garrone, E.; Arean, C. O., Variable temperature infrared spectroscopy: A convenient tool for studying the thermodynamics of weak solid-gas interactions. *Chem Soc Rev.* **2005**, *34*, 846-857.

65. Lambertz, C.; Chernev, P.; Klingan, K.; Leidel, N.; Sigfridsson, K. G. V.; Happe, T.; Haumann, M., Electronic and molecular structures of the active-site h-cluster in [fefe]-hydrogenase determined by site-selective x-ray spectroscopy and quantum chemical calculations. *Chem Sci.* **2014**, *5*, 1187-1203.

66. Noth, J.; Kositzki, R.; Klein, K.; Winkler, M.; Haumann, M.; Happe, T., Lyophilization protects [fefe]-hydrogenases against o-2-induced h-cluster degradation. *Sci Rep-Uk.* **2015**, *5*.

67. Stripp, S.; Sanganas, O.; Happe, T.; Haumann, M., The structure of the active site h-cluster of [fefe] hydrogenase from the green alga chlamydomonas reinhardtii studied by x-ray absorption spectroscopy. *Biochemistry-Us.* **2009**, *48*, 5042-5049.

68. Pelmenschikov, V.; Birrell, J. A.; Pham, C. C.; Mishra, N.; Wang, H. X.; Sommer, C.; Reijerse, E.; Richers, C. P.; Tamasaku, K.; Yoda, Y.; Rauchfuss, T. B.; Lubitz, W.; Cramer, S. P., Reaction coordinate leading to h-2 production in [fefe]-hydrogenase identified by nuclear resonance vibrational spectroscopy and density functional theory. *J Am Chem Soc.* **2017**, *139*, 16894-16902.

69. Greening, C.; Biswas, A.; Carere, C. R.; Jackson, C. J.; Taylor, M. C.; Stott, M. B.; Cook, G. M.; Morales, S. E., Genomic and metagenomic surveys of hydrogenase distribution indicate h-2 is a widely utilised energy source for microbial growth and survival. *Isme J.* **2016**, *10*, 761-777.

70. Kertess, L.; Adamska-Venkatesh, A.; Rodriguez-Macia, P.; Rudiger, O.; Lubitz, W.; Happe, T., Influence of the [4fe-4s] cluster coordinating cysteines on active site maturation and catalytic properties of c. Reinhardtii [fefe]-hydrogenase. *Chem Sci.* **2017**, *8*, 8127-8137.

71. Land, H.; Senger, M.; Berggren, G.; Stripp, S. T., Current state of [fefe]-hydrogenase research: Biodiversity and spectroscopic investigations. *ACS Catal.* **2020**, *10*, 7069−7086.

72. Duan, J. F.; Mebs, S.; Laun, K.; Wittkamp, F.; Heberle, J.; Happe, T.; Hofmann, E.; Apfel, U. P.; Winkler, M.; Senger, M.; Haumann, M.; Stripp, S. T., Geometry of the catalytic active site in [fefe]-hydrogenase is determined by hydrogen bonding and proton transfer. *Acs Catal.* **2019**, *9*, 9140-9149.

73. Artz, J. H.; Mulder, D. W.; Ratzloff, M. W.; Lubner, C. E.; Zadvornyy, O. A.; LeVan, A. X.; Williams, S. G.; Adams, M. W. W.; Jones, A. K.; King, P. W.; Peters, J. W., Reduction potentials of [fefe]-hydrogenase accessory iron-sulfur clusters provide insights into the energetics of proton reduction catalysis. *J Am Chem Soc.* **2017**, *139*, 9544-9550.

74. Simmons, T. R.; Berggren, G.; Bacchi, M.; Fontecave, M.; Artero, V., Mimicking hydrogenases: From biomimetics to artificial enzymes. *Coordin Chem Rev.* **2014**, *270*, 127-150.

75. Filippi, G.; Arrigoni, F.; Bertini, L.; De Gioia, L.; Zampella, G., Dft dissection of the reduction step in h-2 catalytic production by [fefe]-hydrogenase-inspired models: Can the bridging hydride become more reactive than the terminal isomer? *Inorg Chem.* **2015**, *54*, 9529-9542.

76. Loscher, S.; Schwartz, L.; Stein, M.; Ott, S.; Haumann, M., Facilitated hydride binding in an fe-fe hydrogenase active-site biomimic revealed by x-ray absorption spectroscopy and dft calculations. *Inorg Chem.* **2007**, *46*, 11094-11105.

77. Reijerse, E.; Adamska, A.; Siebel, J.; Weber, K.; Lubitz, W.; Lambertz, C.; Esselborn, J.; Happe, T.; Simmons, T.; Berggren, G.; Artero, V.; Fontecave, M., Spectroscopic and electrochemical characterization of non-native cofactors in [fefe] hydrogenase from chlamydomonas reinhardtii. *Journal of Biological Inorganic Chemistry.* **2014**, *19*, S269-S269.

78. Mulder, D. W.; Ratzloff, M. W.; Bruschi, M.; Greco, C.; Koonce, E.; Peters, J. W.; King, P. W., Investigations on the role of proton-coupled electron transfer in hydrogen activation by [fefe]-hydrogenase. *J Am Chem Soc.* **2014**, *136*, 15394-15402.

79. Pelmenschikov, V.; Birrell, J. A.; Pham, C. C.; Mishra, N.; Wang, H.; Sommer, C.; Reijerse, E.; Richers, C. P.; Tamasaku, K.; Yoda, Y.; Rauchfuss, T. B.; Lubitz, W.; Cramer, S. P., Reaction coordinate leading to h2 production in [fefe]-hydrogenase identified by nuclear resonance vibrational spectroscopy and density functional theory. *J Am Chem Soc.* **2017**, *139*, 16894-16902.

80. Reijerse, E. J.; Pham, C. C.; Pelmenschikov, V.; Gilbert-Wilson, R.; Adamska-Venkatesh, A.; Siebel, J. F.; Gee, L. B.; Yoda, Y.; Tamasaku, K.; Lubitz, W.; Rauchfuss, T. B.; Cramer, S. P., Direct observation of an iron-bound terminal hydride in [fefe]-hydrogenase by nuclear resonance vibrational spectroscopy. *J Am Chem Soc.* **2017**, *139*, 4306-4309.

81. Pham, C. C.; Mulder, D. W.; Pelmenschikov, V.; King, P. W.; Ratzloff, M. W.; Wang, H.; Mishra, N.; Alp, E. E.; Zhao, J.; Hu, M. Y.; Tamasaku, K.; Yoda, Y.; Cramer, S. P., Terminal hydride species in [fefe]-hydrogenases are vibrationally coupled to the active site environment. *Angew Chem Int Ed Engl.* **2018**, *57*, 10605-10609.

82. Trueblood, K. N.; Burgi, H. B.; Burzlaff, H.; Dunitz, J. D.; Gramaccioli, C. M.; Schulz, H. H.; Shmueli, U.; Abrahams, S. C., Atomic displacement parameter nomenclature - report of a subcommittee on atomic displacement parameter nomenclature. *Acta Crystallographica Section A.* **1996**, *52*, 770-781.

83. Dalba, G.; Fornasini, P., Exafs debye-waller factor and thermal vibrations of crystals. *J Synchrotron Radiat.* **1997**, *4*, 243-255.

84. Styring, S.; Rutherford, A. W., Deactivation kinetics and temperature-dependence of the s-state transitions in the oxygen-evolving system of photosystem-ii measured by electron-paramagnetic-res spectroscopy. *Biochimica Et Biophysica Acta.* **1988**, *933*, 378-387.

85. Hedison, T. M.; Shanmugam, M.; Heyes, D. J.; Edge, R.; Scrutton, N. S., Active intermediates in copper nitrite reductase reactions probed by a cryotrapping-electron paramagnetic resonance approach. *Angew Chem Int Edit.* **2020**.

86. Guo, Z.; Lin, S.; Xin, Y. Y.; Wang, H. Y.; Blankenship, R. E.; Woodbury, N. W., Comparing the temperature dependence of photosynthetic electron transfer in chloroflexus aurantiacus and rhodobactor sphaeroides reaction centers. *J Phys Chem B.* **2011**, *115*, 11230-11238.

87. Lichtenegger, H.; Doster, W.; Kleinert, T.; Birk, A.; Sepiol, B.; Vogl, G., Heme-solvent coupling: A mossbauer study of myoglobin in sucrose. *Biophys J.* **1999**, *76*, 414-22.

88. Parak, F. G.; Achterhold, K.; Croci, S.; Schmidt, M., A physical picture of protein dynamics and conformational changes. *J Biol Phys.* **2007**, *33*, 371-87.

89. Parak, F.; Frolov, E. N.; Kononenko, A. A.; Mossbauer, R. L.; Goldanskii, V. I.; Rubin, A. B., Evidence for a correlation between the photoinduced electron-transfer and dynamic properties of the chromatophore membranes from rhodospirillum-rubrum. *Febs Lett.* **1980**, *117*, 368-372.

90. Garbers, A.; Reifarth, F.; Kurreck, J.; Renger, G.; Parak, F., Correlation between protein flexibility and electron transfer from q(a)(-center dot) to q(b) in psii membrane fragments from spinach. *Biochemistry-Us.* **1998**, *37*, 11399-11404.

91. Tournier, A. L.; Xu, J. C.; Smith, J. C., Translational hydration water dynamics drives the protein glass transition. *Biophys J.* **2003**, *85*, 1871-1875.

92. Sokolov, A. P., Why the glass transition is still interesting. *Science.* **1996**, *273*, 1675-1676.

93. Cornish, A. J.; Gartner, K.; Yang, H.; Peters, J. W.; Hegg, E. L., Mechanism of proton transfer in [fefe]-hydrogenase from clostridium pasteurianum. *Journal of Biological Chemistry.* **2011**, *286*, 38341-38347.

94. Sode, O.; Voth, G. A., Electron transfer activation of a second water channel for proton transport in [fefe]-hydrogenase. *J Chem Phys.* **2014**, *141*.

95. Siebel, J. F.; Adamska-Venkatesh, A.; Weber, K.; Rumpel, S.; Reijerse, E.; Lubitz, W., Hybrid [fefe]-hydrogenases with modified active sites show remarkable residual enzymatic activity. *Biochemistry-Us.* **2015**, *54*, 1474-83.

96. Winkler, M.; Esselborn, J.; Happe, T., Molecular basis of [fefe]-hydrogenase function an insight into the complex interplay between protein and catalytic cofactor. *Bba-Bioenergetics.* **2013**, *1827*, 974-985.

## TOC Graphic

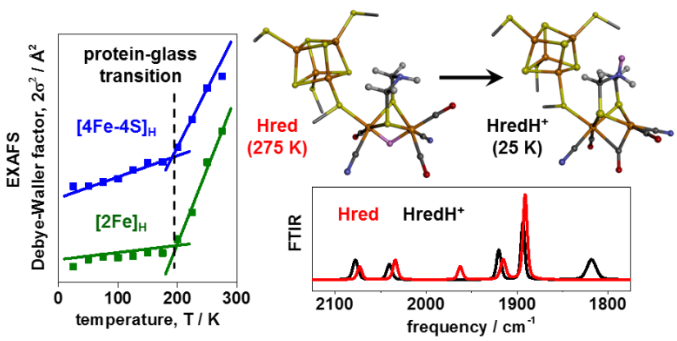


Infrared and X-ray absorption spectroscopy data of [FeFe]-hydrogenases in the cryogenic to ambient temperature range were assayed and evaluated by quantum chemistry. Reduced H-cluster states with a bridging hydride are replaced by states with a bridging CO and a proton at the azadithiolate upon temperature lowering. Impaired ligand rearrangement at the diiron site reflects the protein-glass transition around 200 K. Site-selective proton-coupled electron transfer at the cofactor is essential for $H_2$ conversion in the [FeFe]-hydrogenases.